technische universiteit eindhoven

Faculteit Technische Natuurkunde
Groep Transportfysica
Gebouw Cascade
Postbus 513
5600 MB Eindhoven

Titel: **Simulating relative humidity profiles in the tropics with a high resolution regional meteorological model**

Auteur: Stijn Maas

Verslagnummer: R-1666-A

Datum: januari, 2005

Begeleiders : Dr. P. van Velthoven (KNMI)
Prof.dr. H. Kelder (Tu/e,KNMI)

Simulating relative humidity profiles in the tropics with a high resolution regional meteorological model

S. Maas

Supervisors:
dr. P. van Velthoven (KNMI)
prof. dr. H.M. Kelder (TU/e, KNMI)

Contents

1 Introduction **3**

2 Background **4**
2.1 Water vapor in the atmosphere 4
2.1.1 Role of water vapor in the atmosphere 5
2.1.2 Humidity variables 7
2.2 Water vapor in the tropics 8
2.2.1 Paramaribo Station 9
2.2.2 Climatology of Paramaribo 10
2.3 This study 10

3 Description of models and measurements **13**
3.1 Atmospheric Modeling 13
3.1.1 Basic equations 13
3.1.2 Parametrization of physical processes 14
3.1.3 Spatial resolution 14
3.1.4 Boundary and initial conditions 15
3.2 The model of the European Center for Medium-Range Weather Forecasts (ECMWF) 15
3.3 The Weather Research Forecast model (WRF) 17
3.3.1 Initialization of WRF and running WRF 19
3.4 Measurements: the Snow White (SW) instrument 19

4 Model results **21**
4.1 Evaluation of the WRF-model simulations against the ECMWF analysis . . 21
4.1.1 RH and wind fields 23
4.1.2 Cloud cover 30
4.2 Water vapor profiles 32
4.2.1 Extraction and interpolation method 32
4.2.2 Qualitative comparison of modeled and observed H_2O profiles at WRF levels 33
4.3 Analysis in terms of correlation 38
4.3.1 Correlation between WRF forecasts and observations and between ECMWF analyses and observations 39
4.3.2 Correlation between WRF forecasts and observations and ECMWF forecasts and observations 42
4.4 Influence of miscellaneous variables on the correlation coefficient 46
4.4.1 Influence of interpolation at WRF levels on correlation between ECMWF analyzes and observations 46
4.4.2 Influence of the grid resolution of the boundary values from ECMWF on the WRF simulations 47
4.4.3 Dependence of the correlations on the WRF simulation length . . . 48

5 Summary and Outlook **50**
5.1 Summary 50
5.2 Outlook 50

Acknowledgements **51**

Bibliography **53**

A Results Continued **54**
A.1 ECMWF Forecasts fields and profiles 54
A.2 Correlation significance plots 62

B Programs **64**
B.1 Interpolation Programs 64
B.2 Correlation Programs 67

C WRF namelist **72**

Chapter 1

Introduction

In Surinam, KNMI is coordinating a European research program, STAR (Support for Tropical Atmospheric Research). This program has the objective to improve the knowledge about the composition and dynamics of the tropical atmosphere. As part of this research program water vapor sounding campaigns are performed. A new type state-of-the-art water vapor sensor is being used during these campaigns.

In order to improve the understanding of these observations and the processes governing the vertical water vapor distribution, the water vapor profiles have to be modeled. We will use two models to do this. The model of the European Center for Medium-Range Weather Forecasts (ECMWF) which has a low horizontal resolution, and the Weather Research Forecast (WRF) model which has a high horizontal resolution. The WRF-model is compiled during this study and adapted for initialization with data from the ECMWF. We will compare the output of the two models with the observations.

The main research questions addressed by this work are:

- Which model is most suitable to forecast the observed water vapor distribution?
- Which parameters influence the model results and to what extent?
- In terms of correlation which model preforms the best?

Chapter 2

Background

2.1 Water vapor in the atmosphere

The Earth's atmosphere is a comparatively thin layer of a gaseous mixture which is distributed almost uniformly over the surface of the Earth. In the vertical direction more than 90 % of the mass of the atmosphere is found below an altitude of only 20 km. In comparison, the horizontal dimensions of the atmosphere may be represented by the distance between the north and south poles, and is of the order of 20000 km. If proportions were preserved, the thickness of the atmosphere would be represented on an ordinary office globe by scarcely more than the thickness of a coat of paint. [Sal96]

The atmosphere can be divided into several layers which differ in composition, temperature and stability. Starting from the surface, the main layers are the troposphere, stratosphere, mesosphere and thermosphere, separated by conceptual boundaries called pauses (e.g. tropopause, the boundary between the troposphere and the stratosphere). (see Figure 2.1)

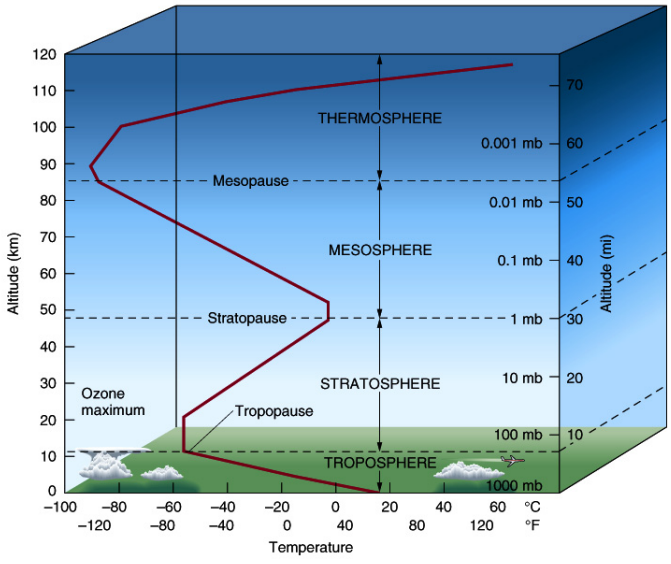

Figure 2.1: Structure of the atmosphere

In spite of its small relative mass and thickness, the atmosphere constitutes the central component of the climatic system. It shows an impressive amount of detail and great variability of its properties both in time and space.

The atmosphere is composed of a mixture of gases, predominantly molecular nitrogen (78% by volume) and molecular oxygen (21% by volume). The remaining 1% volume of the atmosphere consists of trace species like water vapor, argon, carbon dioxide and ozone. Table 2.1 shows the atmospheric composition.

Constituent	Tropospheric mixing ratio
N_2	0.7808
O_2	0.2095
H_2O	$\leq$ 0.040
Ar	0.0093
CO_2	345 ppmv
O_3	10 ppmv
CH_4	1.6 ppmv
N_2O	350 ppbv
CO	70 ppbv
NO	0.1 ppbv
CFC-11, CFC-12	0.2 ppbv

Table 2.1: Chemical composition (by volume mixing ratio) of the troposphere

Most of the constituents, N_2, O_2 and inert gases, are equally distributed up to the mesosphere. Contrary to these constituents the concentration water vapor, H_2O is highly variable especially in the troposphere. It varies between 0% and 4% by volume. It decreases strongly with increasing altitude in the troposphere and increases again slightly in the stratosphere. The main processes controlling the humidity concentration are evaporation, condensation and precipitation, transport and production by CH_4 oxidation.

2.1.1 Role of water vapor in the atmosphere

Water vapor plays a key role in the main energetic and chemical properties of the Earth's atmosphere. Due to the high variability of its concentration in the troposphere, water vapor is one of the most difficult variables to describe and simulate in numerical models of the atmosphere.

Radiative role, water vapor as a greenhouse gas

Water vapor plays an important role in the energy balance and the greenhouse effect of the atmosphere. The surface temperature is highly dependent on the optical depth of the atmosphere which mainly depends, besides other greenhouse gases such as carbon dioxide and ozone on the water vapor pressure. It introduces a positive feedback, the so-called water vapor feedback. The surface temperature determines the maximum of possible water vapor content of the atmosphere (saturation vapor pressure). An increase of the surface temperature can sharply increase the water vapor content and this will lead to an increased optical depth, which further increases the surface temperature. The increase of temperature increases the saturation vapor pressure and

the water content of the atmosphere, and so forth. Therefore H_2O is a greenhouse gas.

Several feedbacks among this positive feedback result in an increase of the main surface temperature with 33^o. This natural greenhouse effect is essential for life on earth. In combination with the clouds, this effect influences the Earth's energy balance, in an order of magnitude greater than that of CO_2.

Chemical role

H_2O is important in many chemical reactions in the atmosphere and especially in the upper troposphere and lower stratosphere, where it plays a role in both ozone formation and destruction [BOT99]. Water vapor is the main source of hydrogen radicals (OH) in the troposphere. OH is formed by reaction of water vapor with excited O ^1D atoms.

$$O(^1D) + H_2O \rightarrow 2OH \tag{2.1}$$

O (^1D) is generated by the photolysis of ozone:

$$O_3 + h\nu \rightarrow O(^1D) + O_2 \tag{2.2}$$

OH is the main cleansing agent in the atmosphere and determines its oxidation capacity. For example, reaction with OH is the main removal mechanism for most hydrocarbons (reaction 2.3) and CO:

$$OH + CH_4 \rightarrow H_2O + CH_3 \tag{2.3}$$
$$OH + CO \rightarrow H + CO_2 \tag{2.4}$$

In part of the stratosphere, ozone destruction is governed by reaction with $HO_x(= OH + HO_2)$

$$HO_2 + O_3 \rightarrow OH + 2O_2 \tag{2.5}$$
$$OH + O_3 \rightarrow HO_2 + O_2 \tag{2.6}$$

Cloud formation

Water vapor in the tropics plays a key role in regulating the temperature in the so-called thermostat hypothesis put forward by Ramanthan and Collins (1991) [RC91] Increased sea surface temperatures (SST) lead to increased evaporation especially near the equator, triggering the formation of deep convective clouds with associated extensive cirrus outflow. These high cirrus clouds shield the radiation from the sun leading to a cooling of the sea surface. This is therefore a negative cloud feedback.

Contrary to this negative feedback during the day of high cirrus clouds in the tropics, low clouds have a positive effect on the surface temperature during the night. They reflect the outgoing LW radiation emitted by the surface, which tempers the surface cooling during the night. During the day they usually have a cooling effect at the surface because they shield the incoming solar radiation.

2.1.2 Humidity variables

As described above atmospheric humidity (the amount of water vapor present in the atmosphere) is important for determining evaporation, atmospheric radiative transfer and certain chemical reactions. To describe the concentration water vapor in the atmosphere the variable relative humidity (RH) is often used. This section deals with the thermodynamic laws which describe this variable.

Air and water vapor closely obey the ideal gas law. The partial pressure, *e*, of water vapor in the atmosphere is given by Dalton's law (the ideal gas law) [Cur03] :

$$e = \rho_v R_v T \tag{2.7}$$

Here ρ_v is the water vapor density (often referred to as the absolute humidity), R_v is the specific gas constant for water, and *T* is the atmospheric temperature. The atmospheric relative humidity is defined as the ratio of the atmospheric vapor pressure to the saturation (or equilibrium) vapor pressure at the temperature of the air, e_s. To determine e_s the phase diagram of water needs to be considered (figure 2.2). This diagram outlines the relation between the three phases (solid, liquid and gas) of water. The existence of the different phases depends on the pressure *p* and

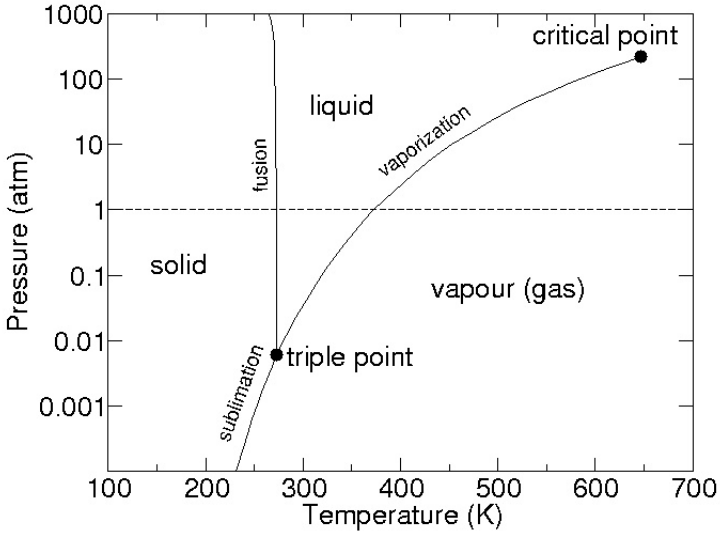

Figure 2.2: Phase diagram of H_2O

the temperature *T*. When the vapor phase is in equilibrium with the liquid phase, the gas is called saturated. In general, the liquid-vapor equilibrium is expressed by the Clausius-Clapeyron equation:

$$\frac{de_s}{dT} = \frac{\delta S}{\delta V} = \frac{L}{T\delta V} \tag{2.8}$$

Where e_s is the saturation pressure, δS is the entropy gained when a unit mass changes from liquid to vapor, δV is the increase of volume during this transition and L is the latent heat of

vaporization per unit mass. This equation can be simplified using the Dalton law (equation 2.7) and the fact that the volume of water vapor per unit mass V_v is much larger than that of liquid water, so δV is about equal to V_v.

$$\frac{de_s}{dT} = \frac{Le_s}{R_v T^2} \tag{2.9}$$

Equation 2.9 states that at any given temperature there is one and only one pressure at which vapor is in equilibrium with liquid water. This saturation pressure increases almost exponentially with increasing temperature.

Integration of equation 2.9 is difficult owing to the variation of the latent heat L of vaporization with temperature. Additionally, application of the Clausius-Clapeyron equation for water vapor (equation 2.9) to determine the saturation vapor pressure e_s in the atmosphere is not strictly valid because of the presence of other gases, and it differs for liquid water and ice. Hence an empirical, numerical equation derived (*ref sonntag*) from equation 2.9, is used to calculate the saturation vapor pressure for both liquid water and ice (indicated by subscripts w respectively i):

$$e_{sw/i} = \exp(a_1 T^{-1} + a_2 + a_3 T + a_4 T^2 + a_5 \ln T) \tag{2.10}$$

The coefficients a_i are presented in tabel 2.2

Coefficient	Liquid water	Ice
a_1	$-6096,9385$	$-6024,5282$
a_2	$16,6358$	$24,7219$
a_3	$-27,1119.10^{-3}$	$10,6139.10^{-3}$
a_4	$16,7395.10^{-6}$	$13,1988.10^{-6}$
a_5	$2,4335$	$-0,4938$

Table 2.2: coefficients of saturation vapor pressure equation 2.10 for both liquid water and ice.

The relative humidity, RH, is defined as

$$RH = \frac{e}{e_{sw}} \tag{2.11}$$

where e_{sw} is the saturation vapor pressure over water.

RH_i, the relative humidity with respect to ice saturation, is defined as

$$RH_i = \frac{e}{e_{si}} \tag{2.12}$$

where e_{si} is the saturation vapor pressure over ice. The relative humidity is commonly multiplied by 100 and thus expressed as percentage.

2.2 Water vapor in the tropics

To understand the global climate system, processes in the tropics merit particular attention. The tropics comprise half of the area of the globe, if we consider that the boundaries of the tropics are roughly at 30^oN and 30^oS. Therefore understanding the dynamics and chemical composition of

the tropical atmosphere are essential for the global climate models.

In the equatorial region, where average solar radiation is greatest, air is warmed at the surface and rises (deep convection). This creates a band of low pressure, centered around the equator. This rising air is replaced by the Trade winds from north and south, so the air from both hemispheres converges in this band. This equatorial band of low pressure is called the Inter Tropical Convergence Zone (ITCZ), see figure 2.5. Figure 2.3 shows the zonal-mean distribution of water

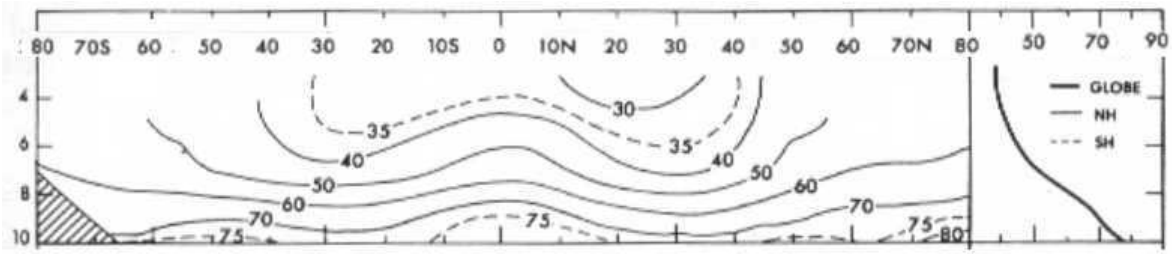

Figure 2.3: Zonal-mean cross sections of the relative humidity in % for annual mean conditions

vapor [PO92]. Most water vapor is found in the equatorial region at the ocean surface. Introduced at the surface of the tropical atmosphere, water vapor is carried aloft by deep convection (strong vertical transport), and horizontal eddies. (figure 2.4)

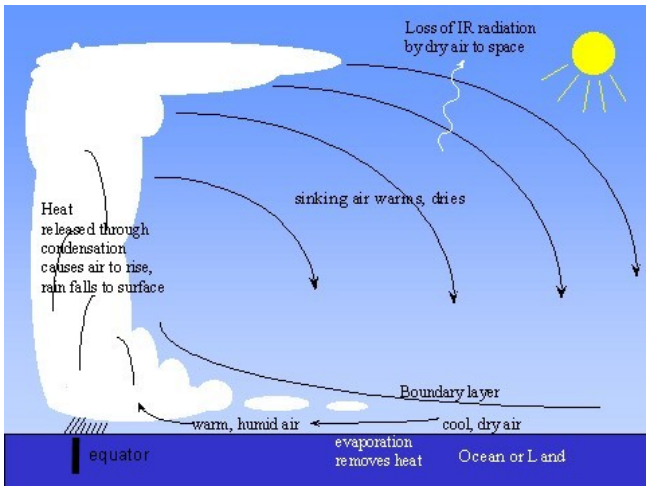

Figure 2.4: Main circulation of water vapor near equator

2.2.1 Paramaribo Station

As stated above the tropics play an important role in the climate of the Earth. Nevertheless observatories in these regions are scarce. One of the few observatories is the Paramaribo station (5.8N and 55.2W) in Surinam. Surinam is of particular interest for atmospheric research in the tropics because of the passing, twice a year, of the ITCZ over Surinam (figure 2.5). This station has been operational since 1999, as a result of a collaboration between the Royal Netherlands Meteorological Service (KNMI) and the Meteorological Service of Surinam (MDS). At the site greenhouse

gases and aerosols are being monitored, and the results are contributed to the Global Atmosphere Watch (GAW) database of the World Meteorological Organization (WMO). Table 2.3 shows the instrumentation of the station and the observed parameters. Besides these continuously observed

Instrument	Parameter
Brewer MKIII	col. O_3, UV Umkher
MAX-DOAS	NO_2, BrO, O_3, ClO
O_3-monitor	O_3 at surface level
Solar Radiation Station	global, direct and diffuse radiation, λ_{int} 300-3000nm
Sunphotometer	Aerosol opt. depth (at 6 diff λ)
Total Sky Imager	total sky cloudiness

Table 2.3: Instrumentation of Paramaribo station

parameters, there is a weekly balloon sounding to measure vertical profiles of O_3, temperature, RH and wind. In addition to these weekly RH-profile measurements made with regular Vaisala RS80 and RS90 humidity sensors, the station is running a program with the Snow White (SW) instrument, chilled-mirror hygrometer. These SW state of the art humidity sensors are sounded on an irregular base. The advantage of the SW over the Vaisala humidity sensors is its accuracy in the upper troposphere and lower stratosphere where the RS sensors lose detail.

2.2.2 Climatology of Paramaribo

Surinam has a typical rain forest climate . Locally the precipitation can be just below the minimum value as defined for a tropical climate (60 mm in the most dry month). The average yearly temperature in Paramaribo is $27,3^o$ C. The daily average maximum temperature is highest in October ($33,0^o$ C) and lowest in January ($29,8^o$ C). During the whole year, the average minimum temperature lies close to 23^o C. The mean relative humidity at surface level, on an annual mean base is 80% and on average 60% of the sky is covered with clouds.

The seasons in Surinam are determined by the annual migration of the Inter Tropical Convergence Zone (ITCZ). [Pet02]. The distinction between the wet and dry seasons is related to the position of the ITCZ. The wet seasons (December-January and April-July) correspond with the period when the ITCZ is located mainly above Surinam. During the dry seasons (February-March and August-November) the ITCZ is located south (Feb-Mar) or north (Aug-Nov) of Surinam. During the second dry season the air transported to Surinam comes from the Southern Hemisphere. From a meteorological point of view, Surinam is located in the Southern Hemisphere during this long dry season. The migration of the ITCZ over Surinam (red spot) is shown in figure 2.5. [Wal03]

2.3 This study

Numerical weather models are used to simulate and predict the global climate and local weather conditions. There are many models, which differ in characteristics such as scale, chemistry and physics. These models are continuously under development and being improved. In these models water vapor distribution is a key element, which is only partly understood due to its high

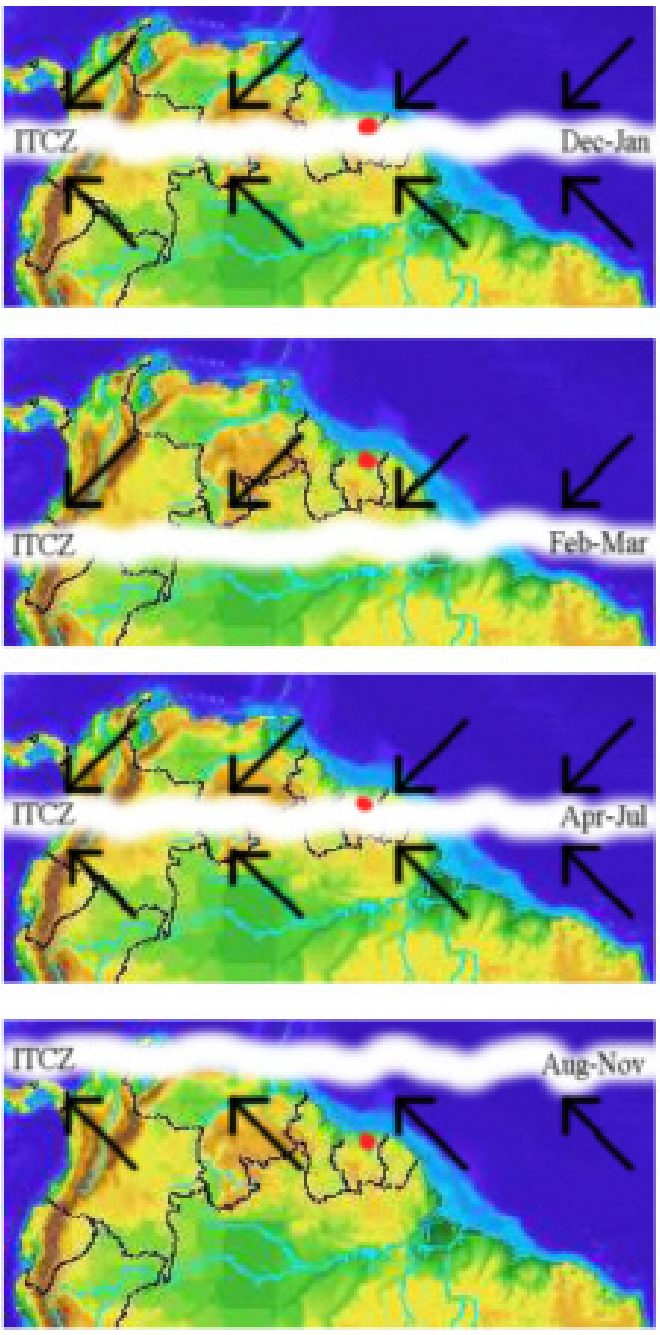

Figure 2.5: migration of ITCZ over Paramaribo

variability in time and space.

This study will compare the observed RH profiles of the SW soundings with the RH profiles generated by two models. The main model used in this study is the new state of the art WRF model, which is still under development. This model is installed and run during this study. The main characteristic of the model is its high horizontal resolution. It is especially developed

for horizontal resolutions in the order of 1km - 10km. Therefore it is a so-called mesoscale model.

The other model used in the study is the global ECMWF model. This model is generally used for weather forecasting and research in Europe and has proven its reliability. The horizontal resolution of the model is approximately 60km by 60km , a so-called large scale model.

Chapter 3

Description of models and measurements

3.1 Atmospheric Modeling

3.1.1 Basic equations

The atmosphere is mathematically described by a closed system of six physical equations with specified boundary conditions [Per03]. Two equations are diagnostic and describe the static relation between different parameters.

- The Ideal Gas Law gives the equation of state for an ideal gas as a relation between pressure P, density ρ, and temperature, T.
$$P = \rho RT \tag{3.1}$$
- The Hydrostatic equation expresses the approximate relationship between the density of the air ρ and the change of pressure with height Z.
$$\frac{\partial p}{\partial z} = -\rho g \tag{3.2}$$

The other four equations are prognostic and describe the changes with time of the wind components *u, v, w,* temperature T, and water vapor content of an air parcel *Q,* and of the surface pressure, P_0.

- The equation of continuity expresses the mass conservation and determines the vertical velocity and change in the surface pressure.
- The equation of motion describes how the momentum of an air parcel changes due to the pressure gradient and the Coriolis force. Included are also the effects of turbulent drag and gravity wave breaking.
- The thermodynamic equation expresses how the change in an air parcel temperature is brought about by adiabatic cooling or warming due to vertical displacements. Other physical processes like condensation, evaporation, turbulent transport and radiative effects are also included.
- The conservation equation for moisture assumes that the moisture content of an air parcel is constant, except for losses due to precipitation and condensation or gains by evaporation from clouds and rain or from the oceans and continents.

Due to the characteristics of these equations, i.e. they are nonlinear partial differential equations, a precise analytical solution is not possible. The method to solve them is to approximate them numerically – classically by iterating to an acceptably close approximation. However nowadays they are being solved simply by discretisation for global models in the spectral domain. This concept is called Numerical Weather Prediction (NWP). [Pet04]

3.1.2 Parametrization of physical processes

The above six basic physical equations describe the main atmospheric model. The atmospheric phenomena described by these equations span a very wide range of scales both in time and space. [Ely02] For instance, general circulation features extend for 1000km or more in space and last for days to weeks whereas boundary layer turbulent flows persist only for a few minutes with dimensions of the order of centimeters to meters. In order to take into account these small-scale disturbances in space and time on the larger scales, explicitly resolved by the model, their effect is being parameterized by including a term in the equations that gives a simplified description of the phenomena. Parametrization is the calculation of the overall effect on a grid cell in terms of known grid scale variables.

The main physical phenomena that are taken into account using parametrization are:

- The orography
- The planetary boundary layer
- The radiation
- The clouds
- The hydrological cycle

3.1.3 Spatial resolution

An important parameter of an atmospheric model is its spatial resolution. In the horizontal direction nowadays the distance between two grid points is usually in the range of 1-10km for mesoscale models (regional models) and 50-100km for global (large-scale) models. Global models use rectangular or Gaussian horizontal grids and sometimes perform part of their calculations in spectral space. Regional models usually operate on a rectangular longitude-latitude grid.

In the vertical direction there are several coordinate systems [PO92] that can be used such as the z system (meter), the θ system (potential temperature), the p system (hPa) and the σ system defined by equation 3.3

$$\sigma = \frac{p - p_t}{p_0 - p_t} \tag{3.3}$$

Here p_0 is the surface pressure and p_t the pressure at the top of the model domain. Presently, most meteorological models use the σsystem or a combination of the σ-system and pressure (hybrid σ-pressure coordinates). With the σsystem the problem of having a vertical coordinate system that intersects the mountains is reduced, because the $\sigma = 1$ surface coincides, even over

mountains, with the Earth's surface. Furthermore, with this system it is easier to incorporate the vertical exchange processes in the planetary boundary layer. At the top of the vertical domain $\sigma = 0$ and at the Earth's surface $\sigma = 1$. However, high up in the stratosphere the influence of the surface is no longer felt. Therefore models with high lids usually make use of pressure coordinates. In the hybrid σ-pressure system there is a smooth transition from σ coordinates near the surface to pressure coordinates in the stratosphere.

3.1.4 Boundary and initial conditions

At the boundaries of a model's domain and at the beginning of a run, we are confronted with a problem: how does the model interpret data that is entering and leaving the domain and what is the condition of the atmosphere in the domain at the start of a run? This is where boundary and initial conditions come into play. They inform the model of the initial atmospheric conditions in the domain and of the state of the air entering the model's domain on the upstream side. This allows the model to accurately compute how the air evolves after it has moved into the domain. In the same way as a forecaster can not accurately make a forecast without analyzing the current conditions, a forecast model can not accurately forecast the atmospheric phenomena without ingesting the initial and boundary conditions.

3.2 The model of the European Center for Medium-Range Weather Forecasts (ECMWF)

The ECMWF was set up in 1975 with the aim of providing weather forecasts for up to several days ahead. These were expected to be of great economical value for the European area. The first aim was to provide 5-day forecasts that had the same accuracy as the 2 day forecasts prepared before the "computer age" set off. This has been achieved and the deterministic forecast now have a validity up to about 8 days ahead. The accuracy varies considerably with time and place. In some circumstances, useful forecasts up to 10 days can be made, at other times they have hardly any predictive accuracy beyond 4 days.

Nowadays the heart of the ECMWF model is the Integrated Forecasting System (IFS), which was developed in collaboration with Météo-France (where it is known as ARPEGE). The basic version of the present model code was taken in operation in March 1994. This code includes all the features required for three-and four-dimensional variational data assimilation, and for determining optimal unstable perturbations for ensemble prediction. However, the model is continuously being updated as improvements become available (several times a year). [Per03]

Spatial resolution
The vertical coordinate system of the ECMWF model is the hybrid σ- pressure system. The vertical resolution of the ECMWF model is highest in the Planetary Boundary Layer (PBL) and lowest in the stratosphere and lower mesosphere. The atmosphere is divided into 60 layers up to 0.1hPa (about 64km). The levels in the lower and middle troposphere are σ-levels which follow the Earth's surface, and in the upper stratosphere and mesosphere surfaces they follow surfaces of constant pressure p. See figure 3.1.

For its horizontal resolution the ECMWF model uses two different numerical representations:

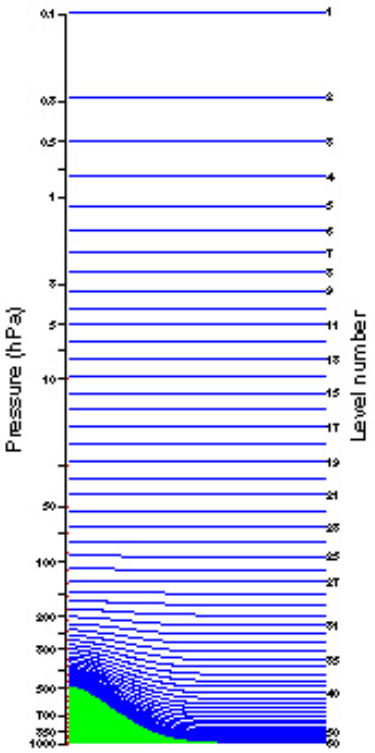

Figure 3.1: vertical levels of ECMWF

The first a *spectral method* is based on a spherical harmonic expansion, truncated at total wave number 511, for the representation of fields and the computation of horizontal derivatives in dynamics computations.
The second is a *grid point representation* used for computing parametrizations of physical processes and the consequent tendencies. The so-called Gaussian grid, is quasi-regular in longitude and almost regular in latitude. Due to the convergence of the longitudes toward the poles, certain cells are merged polewards, so that the east-west radial distance between the points increases polewards, but the geometric distance varies much less. The average geometric distance between the grid points is about 60km.

Analysis
At ECMWF four global analyses per day are produced at 00, 06, 12 and 18UTC. These are obtained by two "four-dimensional variational data assimilation" (4DVAR) minimisation cycles running from 03 to 15 UTC and from 15 to 03 UTC. The analysis is performed by comparing the observations directly with a very short forecast, using exactly the same model as the operational medium-range forecast. The differences between the observed values and the corresponding values predicted by the short-range forecast are used to make a correction to the first-guess field in order to produce the atmospheric analysis. These analyses are used as initial and boundary conditions for the subsequent medium-range forecast model simulations.
Forecasts
ECMWF runs two main forecast suites. One produces global 10-day forecasts based on the 12UTC

analysis. The second one produces global 3-day forecast run four times a day based on the four analyses made each day. A few of the parameters computed in these forecasts are summarized in table 3.1.

ECMWF model variable output
Temperature
Wind (U, V and W components)
Specific humidity

Table 3.1: Primary ECMWF model output variables

These primary parameters can be used to derive other atmospheric parameters like potential vorticity, geopotential height, vorticity and divergence. Apart from these primary parameters, a large number of other surface and atmospheric parameters is archived e.g. cloud cover, that play a role in the parameterizations or that can be diagnosed. All parameters are achieved at 3-hourly intervals from 3 to 72 hours and every 6 hours from 72 to 240 hours.

3.3 The Weather Research Forecast model (WRF)

The Weather Research and Forecast (WRF) is being developed in the USA in a collaborative effort by the National Center for Atmospheric Research (NCAR), the National Center for Environmental Prediction (NCEP), the Forecast Systems Laboratory (FSL), the Air Force Weather Agency (AFWA), Oklahoma University (OU) and other university scientists. The WRF project aims at developing a next-generation mesoscale forecast model and assimilation system that will advance both the understanding and the prediction of mesoscale precipitation systems and will promote closer ties between the research and operational forecasting communities. The model incorporates advanced numerics and data assimilation techniques and improved physics, particularly for dealing with convection and mesoscale precipitation. It is intended for a wide range of applications, from idealized research to operational forecasting, with particular emphasis on horizontal grids of 1-10km. The flowchart of the WRF modeling system is presented in figure 3.2.

The WRF model is a fully compressible, nonhydrostatic model (with a hydrostatic option). Its vertical coordinate is a terrain-following hydrostatic pressure coordinate. The grid staggering is the Arakawa C-grid. The model uses the Runge-Kutta 2nd and 3rd order time integration schemes, and 2nd to 6th order advection schemes in both horizontal and vertical directions. It uses a time-split small step for acoustic and gravity-wave modes. The dynamics conserves scalar variables.

The flowchart illustrates the component programs of the WRF Modeling System. The WRF model can be run with either idealized initialization or real-data initialization. In the used release (release 1.3, 2003), the WRF model supports the Eulerian mass core, referred to as the advanced research WRF (ARW) dynamical core. The purpose of the ideal.F (pink) and real_em.F (blue) programs is to generate input and (if necessary) boundary files for the WRF model. This involves a hydrostatic balance adjustment in addition to setting up the initial 3d and 2d fields of the WRF variables.

The function of the Standard Initialization (green) is to take real-data analyses on another grid, define the WRF horizontal grid, and vertical levels in mass coordinates, generate map, elevation and landuse information for WRF, and horizontally and vertically interpolate fields to the WRF grid. The time-dependent (analysis) fields consist of 3d wind, potential temperature, and water vapor, and a number of 2d fields. [UCA04]

The standard output from SI, real, and WRF model is in netCDF format (one of WRF I/O API format) can be displayed by one or more graphic tools: Vis5D, NCAR Graphics NCL scripts, GrADS, or RIP4. Converters to vis5d, GrADS, and RIP4 data formats are available as are sample NCL scripts that can take netCDF files as input. [NCA04]

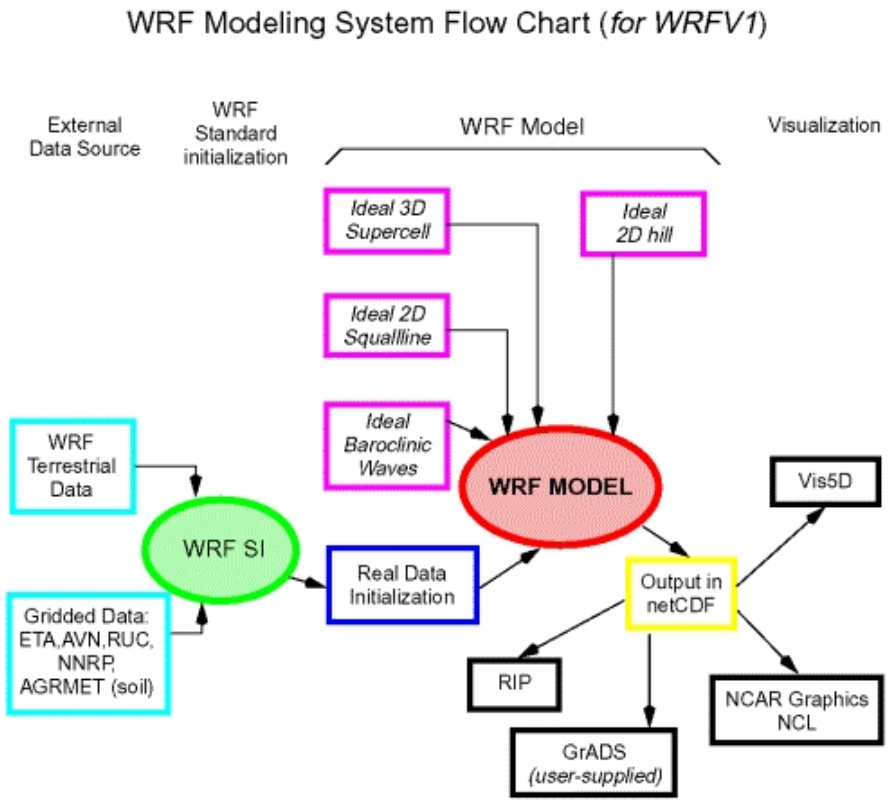

Figure 3.2: The WRF-modeling system

Spatial resolution of WRF
The horizontal grid specified in WRFSI for the domain of the WRF forecasts has a typical resolution of 1-10km. It is because of this high horizontal resolution that WRF is a mesoscale model. The vertical grid of the WRF-model uses η coordinates which are defined by equation 3.4:

$$\eta = \frac{p_h - p_{ht}}{\mu} \qquad where \quad \mu = p_{hs} - p_{ht} \tag{3.4}$$

where p_h is the hydrostatic component of the pressure, and p_{hs} and p_{ht} refer to values along the surface and top boundaries, respectively. This is thus a σ coordinate. The standard number of vertical WRF levels is 31.

3.3.1 Initialization of WRF and running WRF

In this study the WRF-model is only used for real-data cases. Therefore we have to prepare first the initial and boundary conditions from the ECMWF to the wrf input format. This is done by the WRFSI script. But WRFSI is not compatible with the ecmwf-format therefore the data from ecmwf is first preprocessed using an extra FORTRAN-script ecm.f. The output of this program is compatible with WRFSI.

WRFSI has only once to be run completely to determine the location and grid of the domain of interest. After the first completion of WRFSI for the specific domain only the PERL script wrfsi.pl has to be run with the original data for different times. The output of this PERL program is the input for the real program which combines the initial grid conditions and the boundary conditions into the two input files for the wrf program.

The main wrf program can now be ran after adapting the name list, namelist.input, for the specific run. See appendix C

We used WRF version 1.3 and used a forecast length of 48 hours with 6 hourly boundary conditions.

3.4 Measurements: the Snow White (SW) instrument

The observations of water vapor profiles in Paramaribo are executed with the state-of-the-art Snow White sensor. The concept of the SW hygrometer is the chilled-mirror method that is directly based on the thermodynamics, and hence can be regarded as a standard method for measuring the water vapor concentrations. A small mirror (3 mm X 3 mm) exposed to the ambient air is cooled continuously so that its temperature just equals the dew or frost point temperature. A lamp and phototransistor are used to monitor the thickness of the dew or frost layer on the mirror. Figure 3.3

The main advantages of the Snow White hygrometer are as follows:

- SW uses a Peltier cooler, which is a thermoelectric device producing a temperature difference between its two sides. The warm side of the slide Peltier device is cooled by the ambient air, and the mirror attached on the cold side is cooled electrically. SW works with a 9 V dry cell battery (for the control circuit and lamp) and a 1.5 V dry cell battery (for the Peltier cooler and sensor-housing heater). Compared with cryogenic frost point hygrometers, the Snow White may have some difficulty in extremely dry regions of the atmosphere such as the middle stratosphere (less than 3-6 % RH) due to the limitation of the Peltier cooler. However, SW should be capable of measuring water vapor profiles from the surface up to the lower stratosphere. Its advantage is its smaller size so that it can be used during standard balloon soundings.

- Thermocouple thermometry is used for the temperature measurements of SW, and the mirror itself is one of the two contact points of the thermocouple. In other words, the mirror is the thermometer at the same time. Therefore, the error and delay of the temperature measurements are generally small.

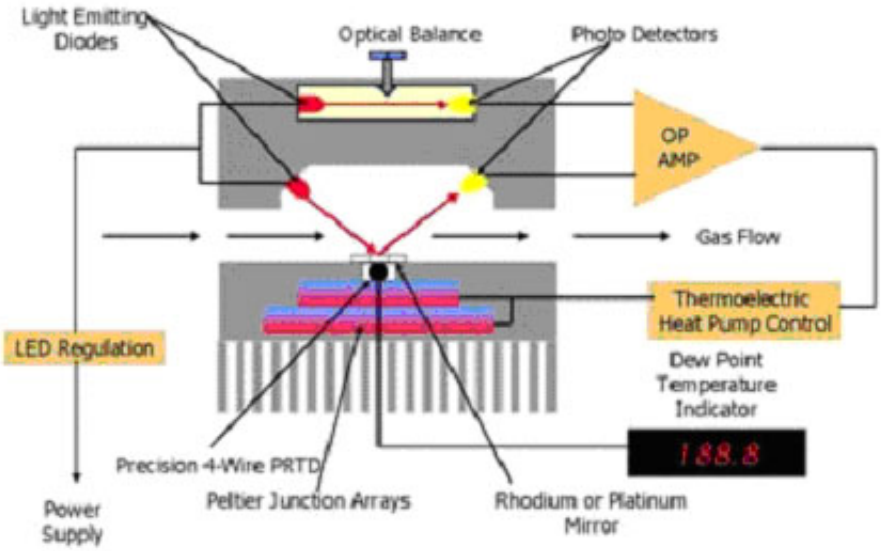

Figure 3.3: Principle of a chilled mirror hygrometer

- One of the characteristics of chilled-mirror sensors is that it is not easy to distinguish between the existence of cloud/particles and the supersaturation. However, with a heater on the sensor housing, SW may be able to provide the information on the total water content in clouds.

Chapter 4

Model results

In chapter 3 the WRF-model is described as well as the ECMWF-model. Here we first show that the results of the WRF-simulations give a realistic description of the state of the atmosphere by comparing them with similar ECMWF-analyses made at coarse resolution.

Secondly we investigate if the WRF-model gives a better representation of the water vapor observations. This is done by calculating correlations between the modeled and observational time series. Correlations between the modeled and observed profiles are also analyzed. To put it briefly we would like to answer the following questions:

- Are the WRF-simulations in agreement with the ECMWF-simulations?
- How do the model simulations compare to satellite observations of clouds?
- Which model performs best in terms of linear correlation between the simulations and observed profiles, WRF or ECMWF?
- What is the influence of interpolation, resolution and forecast length on the correlation coefficient?

4.1 Evaluation of the WRF-model simulations against the ECMWF analysis

As examples of the total model output in the domain of interest (e.g. Surinam) two primary model variables, the water vapor content and the horizontal wind components, are analyzed. Two runs of the WRF-model, i.e. for 1 March 2003 0h UTC and 26 Februari 2004 0h UTC, are qualitatively compared with the ECMWF-analysis at 3 different vertical levels: 700mb (3km), 500mb (5,6km) and 200mb (11,8km). The forecast length of the WRF model simulations is 48 hours. The 6 hourly boundary values and the initial conditions were taken from the ECMWF database using the Meteorological Archival and Retrieval System (MARS).

The horizontal model grid extends in North-South direction from 0^oN till 10^oN and in the East-West direction from 50^oW till 60^oW. In this domain Paramaribo (5.8^oN, 55.2^oW) is located almost exactly at the center of the grid. The number of WRF-grid points in this domain is taken 90X90 resulting in a horizontal resolution of the WRF grid of 14km whereas the number of ECMWF-grid points is 10X10 . The ECMWF grid resolution is about 100km.

To produce the field plots, GrADS (Grid Analysis and Display System) software package has been applied. In order to produce field plots using GrADS, the original WRF-output, which is in the NetCDF-file format (Network Common Data Form), has been converted with the WRF-to-GrADS package (see figure 3.2) to the input format needed by GrADS. The ECMWF-data is already GrADS compatible.

We used the ECMWF analyses in this section to compare with the WRF-forecasts. Because the analyses of ECMWF are a more realistic simulation of the atmosphere than the ECMWF forecasts. The ECMWF forecasts for the same cases are presented in Appendix A.1.

4.1.1 RH and wind fields

Figures 4.1 and 4.2 show the WRF and ECMWF relative humidity at 700mb for 1 March 2003 0h, and Figures 4.3 and 4.4 the corresponding wind vectors. Wind vectors are plotted as barbs. The wind barbs indicate wind direction and speed. They point in the direction the wind is blowing/coming "from". The wind speed is represented by the barbs, each long barb represents 5 m/s and a short barb 2.5m/s. For reasons of readability the wind from WRF is plotted only for one of each 6 grid points.

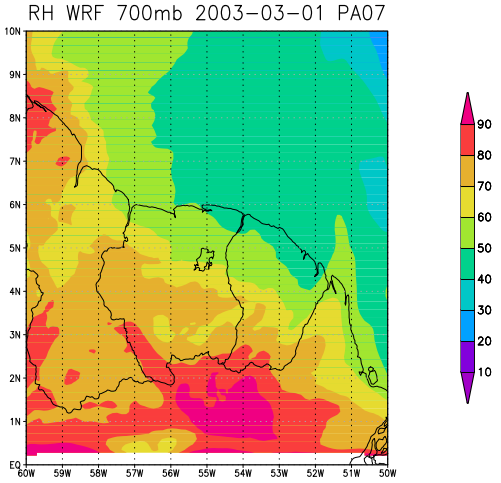

Figure 4.1: RH field at 700mb WRF forecast (48h), on 1 March 2003 00h UTC.

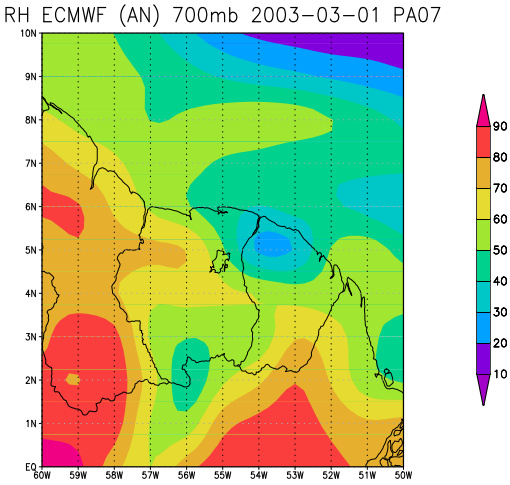

Figure 4.2: RH field at 700mb ECMWF analysis, on 1 March 2003 00h UTC.

The relative humidity distributions show the same large scale structure, however the WRF-model shows more details. The wind field of ECMWF varies only little over this small domain

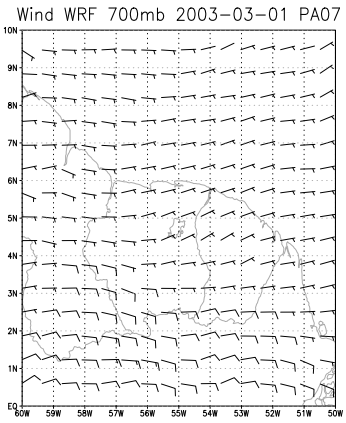

Figure 4.3: Wind field at 700mb WRF forecast (48h), on 1 March 2003 00h UTC

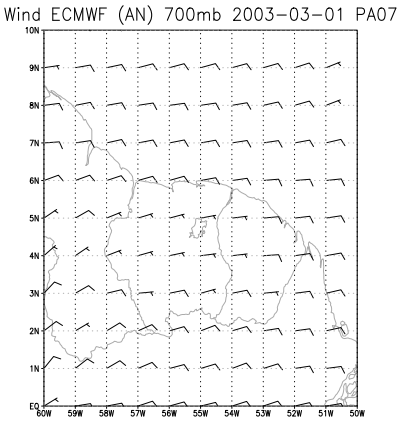

Figure 4.4: Wind field at 700mb ECMWF analysis, on 1 March 2003 00h UTC

but is largely consistent with that from WRF as well. This shows that WRF seems to have been implemented correctly on our computer system.

Figures 4.5and 4.6 show similar plots at 500mb. Again WRF and ECMWF are consistent, but WRF provides more details.

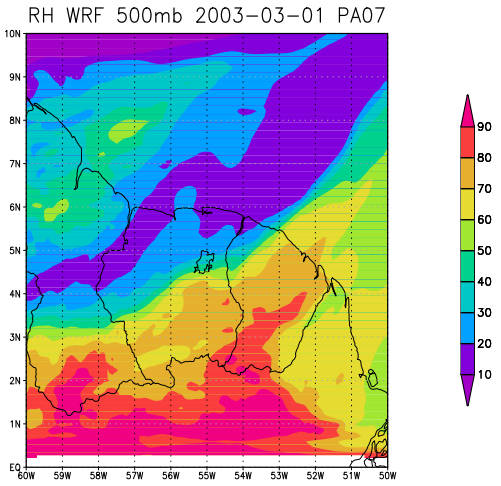

Figure 4.5: As fig. 4.1 but at 500mb

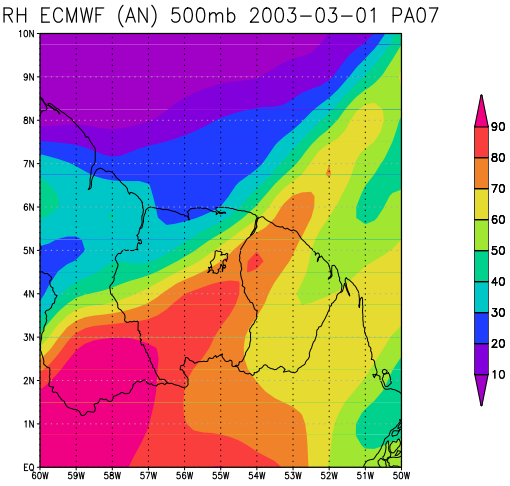

Figure 4.6: As fig. 4.2 but at 500mb

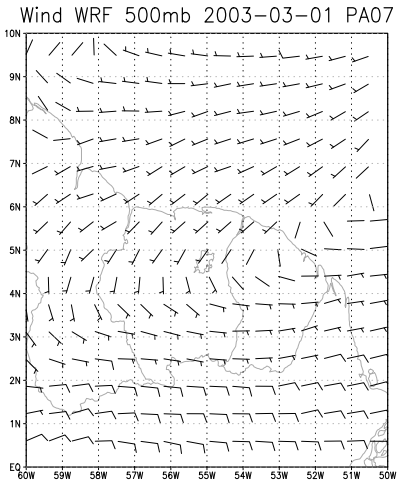

Figure 4.7: As fig. 4.3 but at 500mb

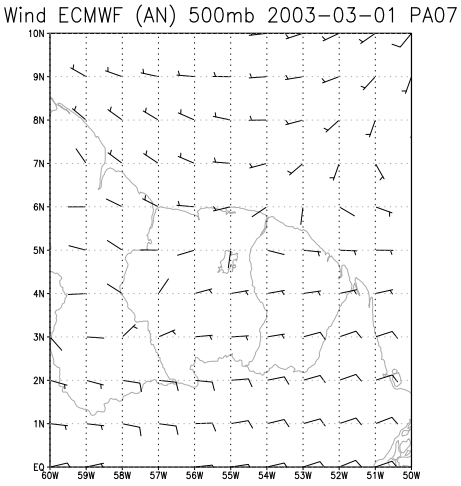

Figure 4.8: As fig. 4.4 but at 500mb

The figures 4.9and 4.10 show the RH-fields at 200mb. In this case the situation is different, the large scale variations in RH differ strongly.

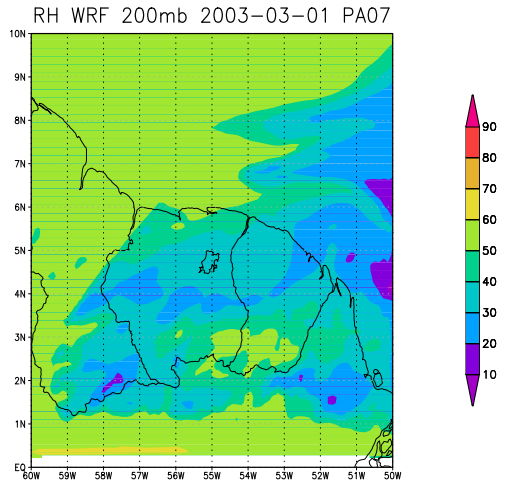

Figure 4.9: As fig. 4.1 but at 200mb

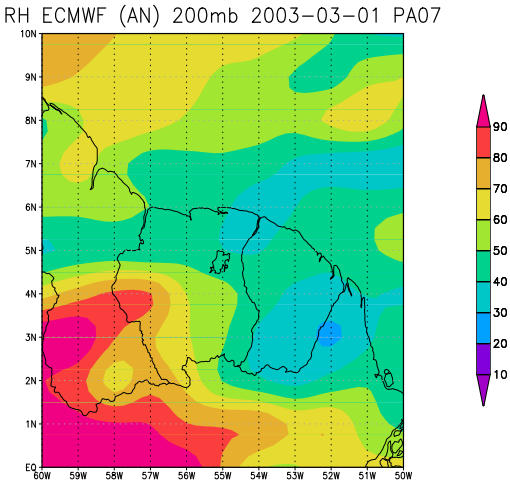

Figure 4.10: As fig. 4.2 but at 200mb

A reason for the larger differences may be the strong variations in RH at upper levels, that are also evident in the balloon soundings that will be shown later. The wind fields figures 4.11and 4.12

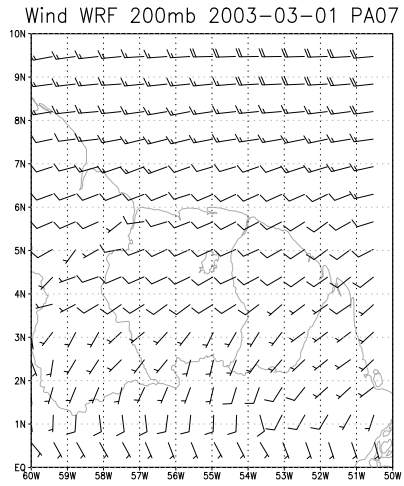

Figure 4.11: As fig. 4.3 but at 200mb

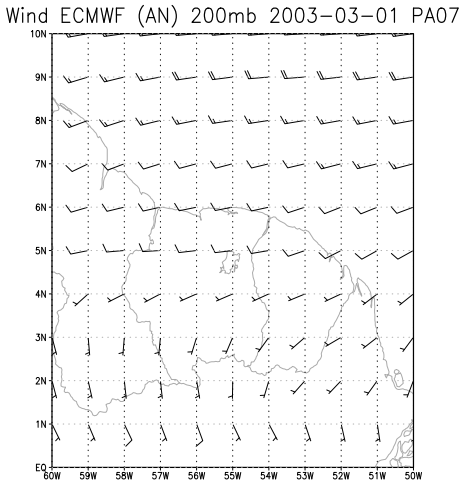

Figure 4.12: As fig. 4.4 but at 200mb

still seem to match quite well.

The next series of figures 4.13 till 4.24 show the RH-fields and wind fields at the same vertical levels as the case before but for 26 February 2004 oh UTC.

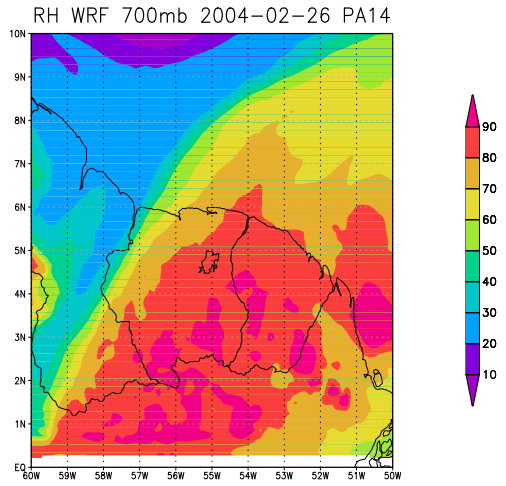

Figure 4.13: RH field at 700mb WRF forecast (48h), on 26 February 2004 oh UTC

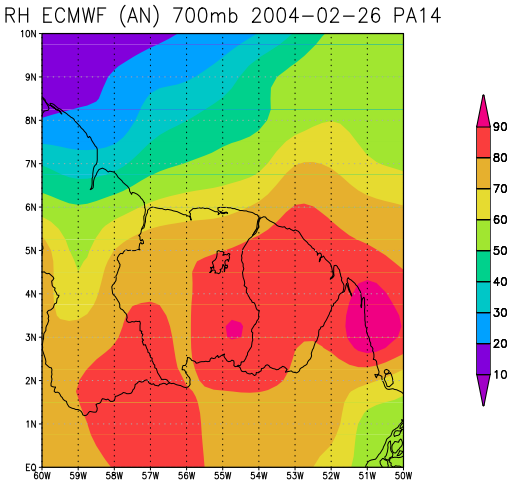

Figure 4.14: RH field at 700mb ECMWF analysis, on 26 February 2004 oh UTC

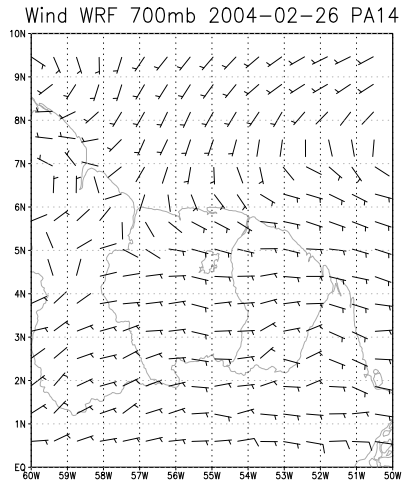

Figure 4.15: Wind field at 700mb WRF forecast (48h), on 26 February 2004 ooh UTC

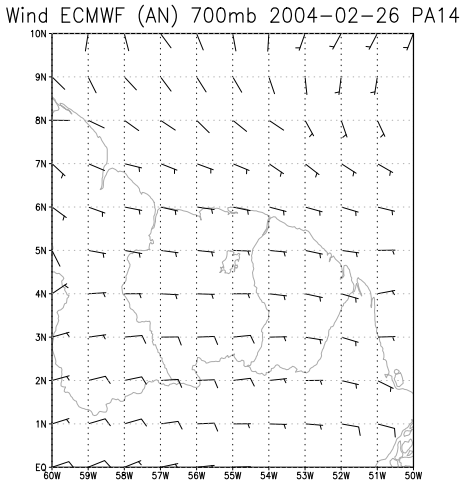

Figure 4.16: Wind field at 700mb ECMWF analysis, on 26 February 2004 ooh UTC

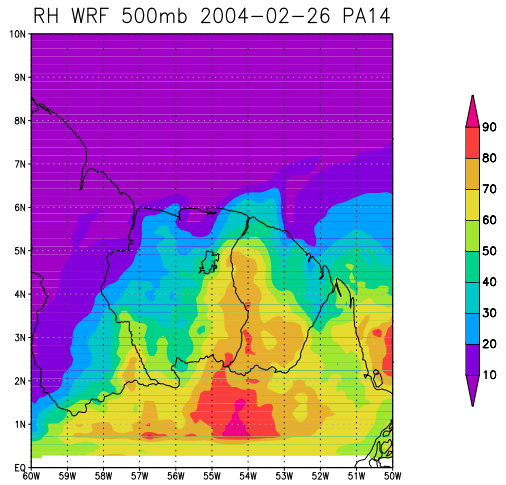

Figure 4.17: As fig. 4.13 but at 500mb

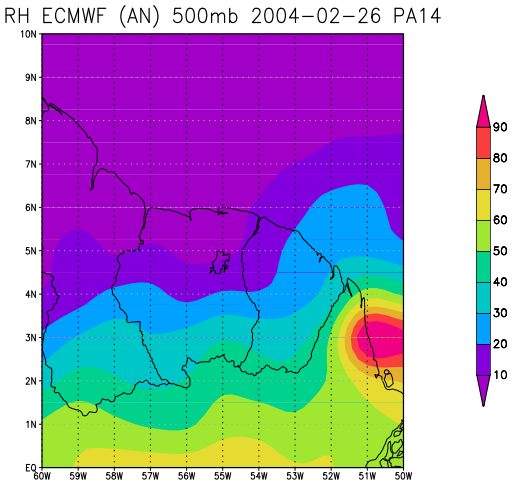

Figure 4.18: As fig. 4.14 but at 500mb

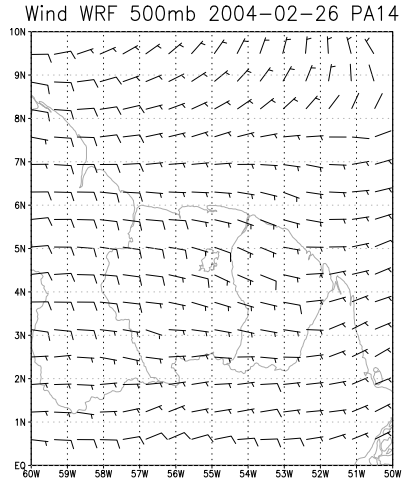

Figure 4.19: As fig. 4.15 but at 500mb

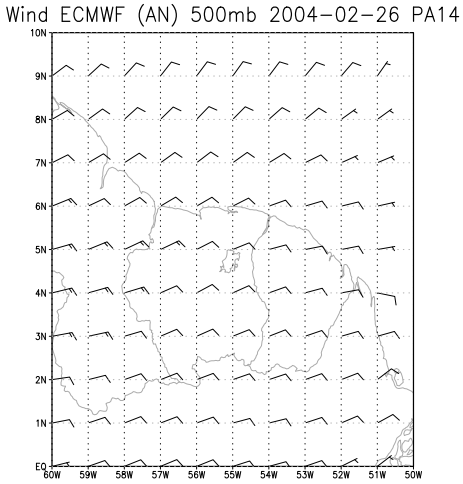

Figure 4.20: As fig. 4.16 but at 500mb

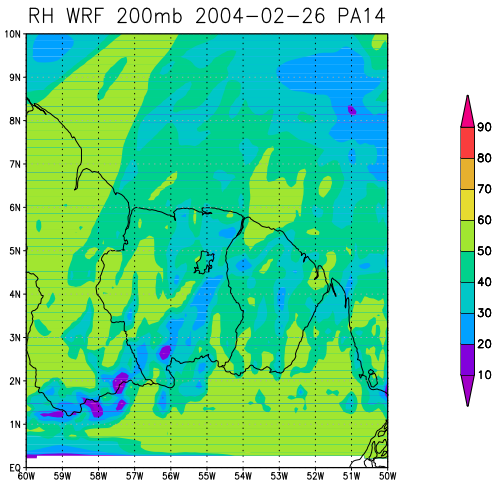

Figure 4.21: As fig. 4.13 but at 200mb

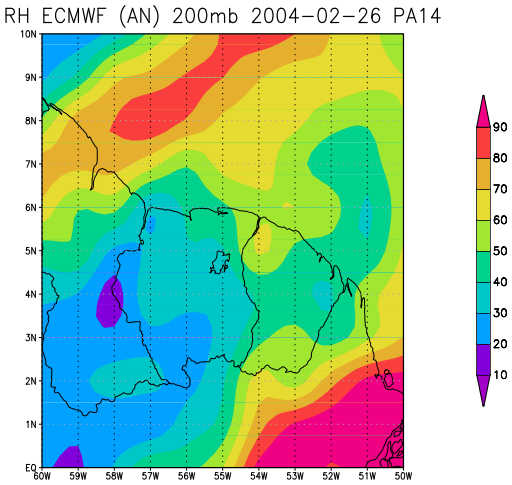

Figure 4.22: As fig. 4.14 but at 200mb

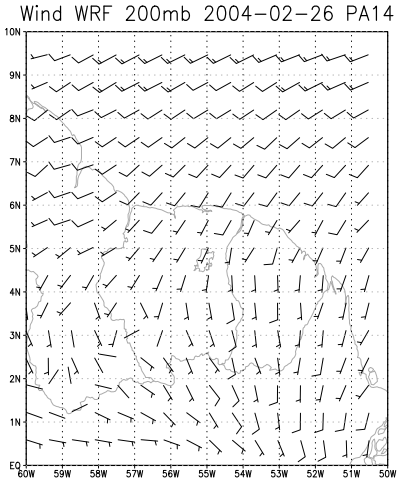

Figure 4.23: As fig. 4.15 but at 200mb

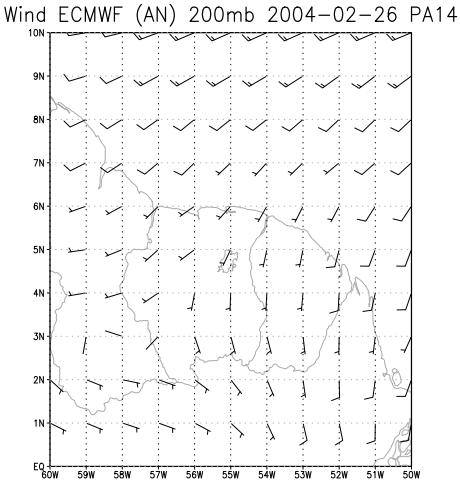

Figure 4.24: As fig. 4.16 but at 200mb

Again the wind fields are consistent for the three levels. The RH-fields show again an anomaly at 200mb whereas the RH-fields at the two lower levels have in general a very similar structure.

The qualitative comparison of the 2 simulations leads to the following conclusions:

- The results show good agreement between the RH fields at low altitudes 700mb and 500mb. However the RH fields at 200mb show significant differences in spatial structure between the two models.
- By and large the wind fields tend to differ usually only slightly. The higher horizontal resolution of the WRF-model results in a more detailed wind field in some cases than represented by ECMWF. Whereas the general directions of both model outputs are in good agreement.

4.1.2 Cloud cover

A parameter that is related to the water vapor content is the cloud cover variable. Clouds occur in saturated parts of the atmosphere (RH=100%). The cloud cover is observed with satellites; one example of these observations is qualitatively compared with the RH field at 500mb of both the models and the high cloud cover variable of the ECMWF model. High cloud cover is defined as all the clouds between 4km and 6km (about 600mb and 450mb).

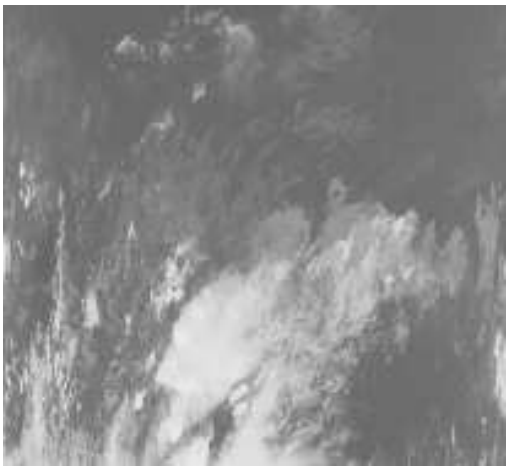

Figure 4.25: Cloud coverage observed on 26 February 2004 00h UTC above Surinam with NOAA-satellite at IR-channel, white colors indicate high clouds.

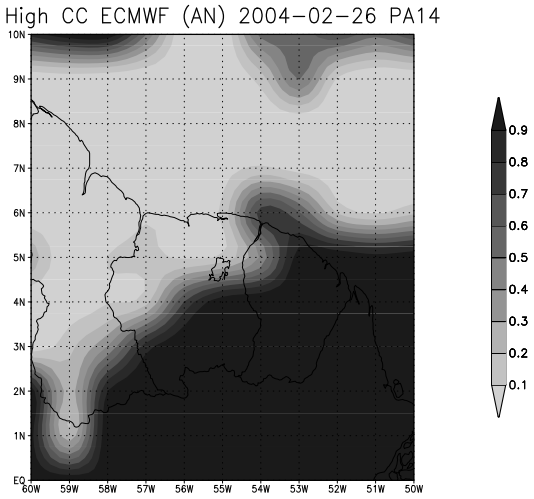

Figure 4.26: High cloud coverage ECMWF analysis on 26 February 2004, 0h UTC. The darkest black color corresponds to a cloud cover of more than 90%.

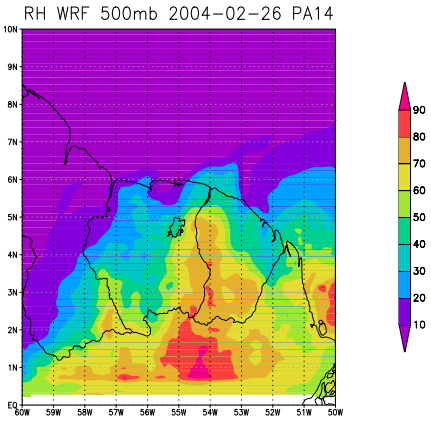

Figure 4.27: As fig. 4.21 but at 500mb

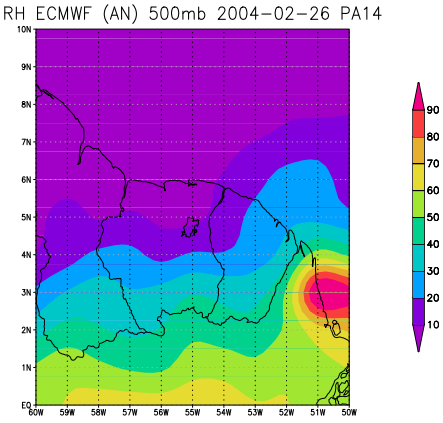

Figure 4.28: As fig. 4.22 but at 500mb

The water vapor distribution of the WRF-forecast apparently shows the best agreement with the observed cloud coverage distribution. The ECMWF-analysis, RH-field and high cloud coverage, show roughly the same pattern but due to the low horizontal resolution, no detailed structures can be distinguished in the ECMWF fields. Besides some agreements between the observations and the modeled fields there are still significant differences between WRF and the satellite observations. Clouds are notoriously difficult to simulate in numerical atmosphere models.

4.2 Water vapor profiles

Here we investigate how well WRF and ECMWF simulate the observed water vapor profiles. The observations of the vertical water vapor distribution above Paramaribo were all done with the SW-sensor. There were three sounding campaigns in Surinam, which resulted in 16 observations of water vapor profiles. In table 4.1 below the dates of the 16 soundings are shown.

flight nr	date	flight nr	date	flight nr	date
PA01	16-10-2002	PA06	29-01-2003	PA12	11-02-2004
PA02	17-10-2002	PA07	28-02-2003	PA13	18-02-2004
PA03	18-10-2002	PA08	31-03-2003	PA14	25-02-2004
PA04	22-10-2002	PA09	30-04-2003	PA15	10-03-2004
PA05	23-10-2002	PA10	30-05-2003	PA16	17-03-2004
		PA11	30-06-2003		

Table 4.1: SW soundings made at Paramaribo station between October 2002 and March 2004

The launch of all sounding balloons took place between 22.15h and 23.00h UTC. The average flight time of the sounding balloons is about 1.5h which makes a comparison with the model simulation at 00h UTC a reasonable choice.

4.2.1 Extraction and interpolation method

Extraction of profiles from model simulations

From all the RH fields (not only at the 3 vertical levels presented in the previous section but for all vertical model levels in the troposphere), we will extract vertical RH profiles at Paramaribo. The top of the vertical domain of WRF st 50mb (19km), leads to 22 vertical WRF levels and correspondingly 38 ECMWF levels. Paramaribo is almost centered in both model domains, this has been done minimize boundary problems.
To obtain the water vapor profiles from the model simulations we used the following methods to extract them from the model output.
For the ECMWF simulations,the RH profiles were calculated from the primarily model variables Q, absolute humidity and T, temperature using equations 2.11, 2.7 and 2.10. These equations are also used in WRF. For the WRF forecasts, the RH profiles were written to the wrf-grads input file,using a FORTRAN script to extract them from the RH-fields.

Interpolation of ECMWF and SW profiles to WRF levels

To make a fair comparison and calculate comparable correlation coefficients between the observed and modeled data, the RH profiles, all have to be on the same vertical grid. To accomplish this, the SW data and the ECMWF data were interpolated to the WRF levels. For this a fortran program (appendix B.1) was written that interpolates the SW values and the ECMWF values between the mid levels of the WRF model using equation 4.1.

$$RH_{wl} = \frac{\sum RH_{i,e/s}[(z_i + z_{i+1})/2 - z_{i,b}]}{\sum[(z_i + z_{i+1})/2 - z_{i,b}]} \tag{4.1}$$

With $RH_{i,e/s}$ the RH value at the SW or ECMWF level z_i and $z_{i,b}$ the bottom mid level of the WRF model. The summation i over all SW or ECMWF levels is between $z_{i,b}$ and $z_{i+1,b}$.

4.2.2 Qualitative comparison of modeled and observed H_2O profiles at WRF levels

Figures 4.29 up to 4.44 show a comparison between the profiles obtained from the SW observations interpolated to the WRF levels, the raw measurements, the ECMWF simulations interpolated at WRF levels and the WRF simulations.

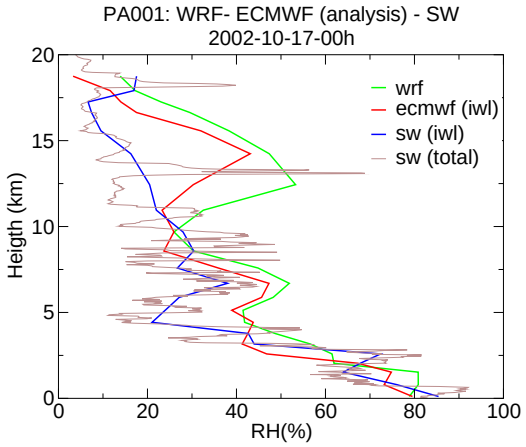

Figure 4.29: profiles of RH at Paramaribo on 17 October 2002 0h UTC from the WRF model (green), ECMWF model (red) and SW (blue) interpolated to the WRF levels, the brown line shows the raw SW data

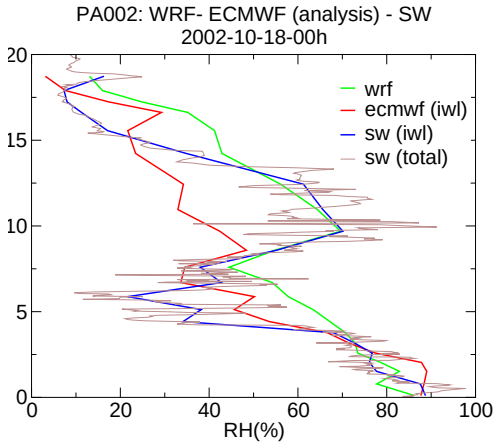

Figure 4.30: As figure 4.29 but on 18 October 2002

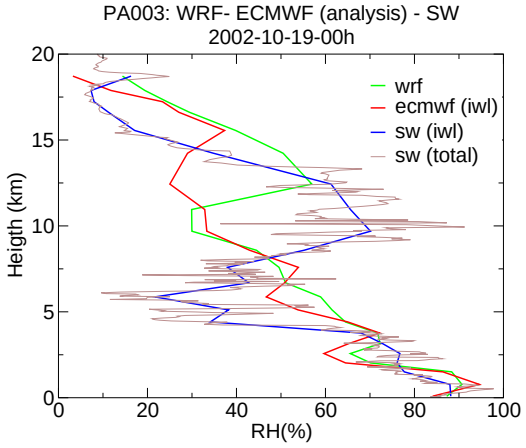

Figure 4.31: As figure 4.29 but on 19 October 2002

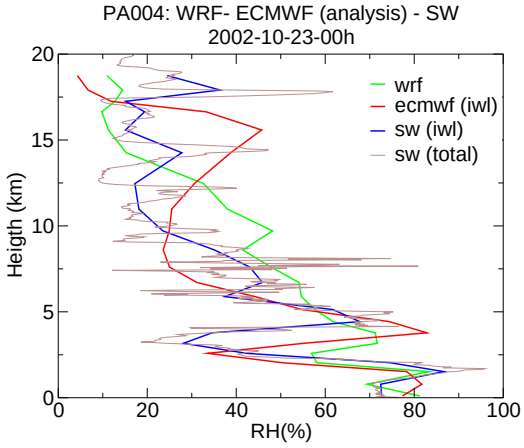

Figure 4.32: As figure 4.29 but on 23 October 2002

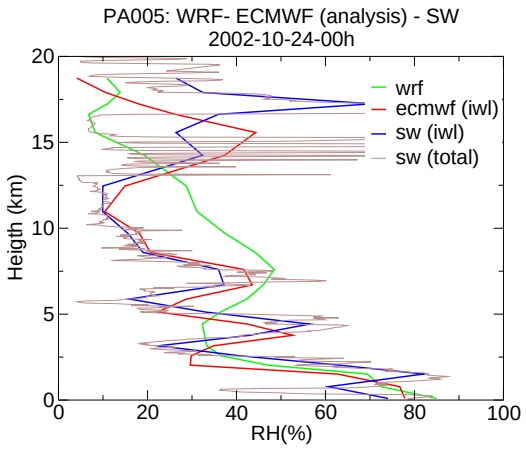

Figure 4.33: As figure 4.29 but on 24 October 2002

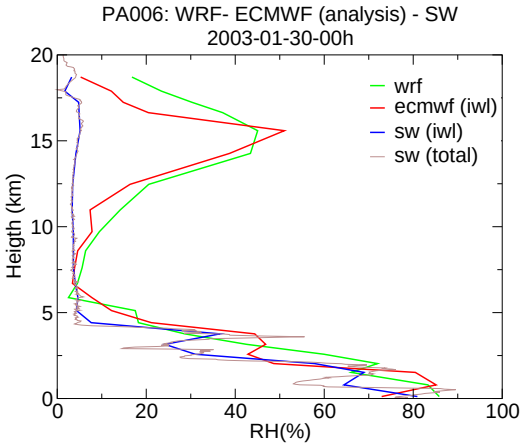

Figure 4.34: As figure 4.29 but on 30 Januari 2003

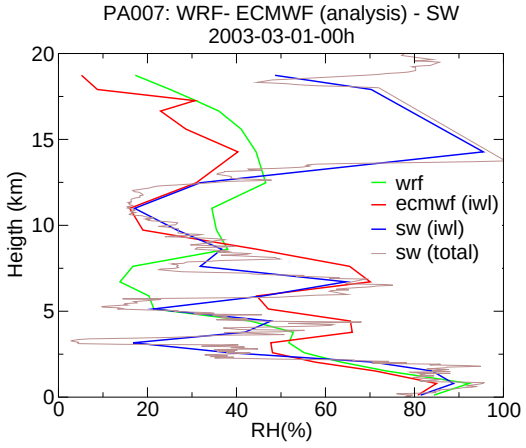

Figure 4.35: As figure 4.29 but on 1 March 2003

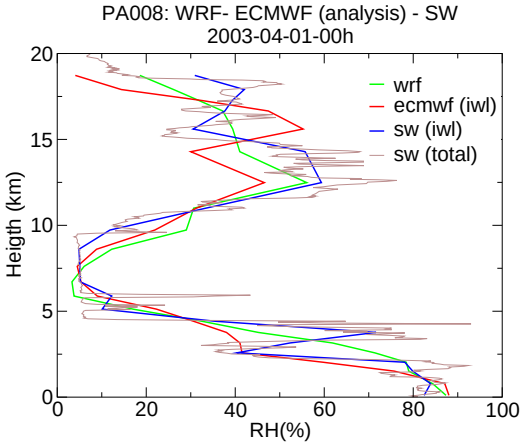

Figure 4.36: As figure 4.29 but on 1 April 2003

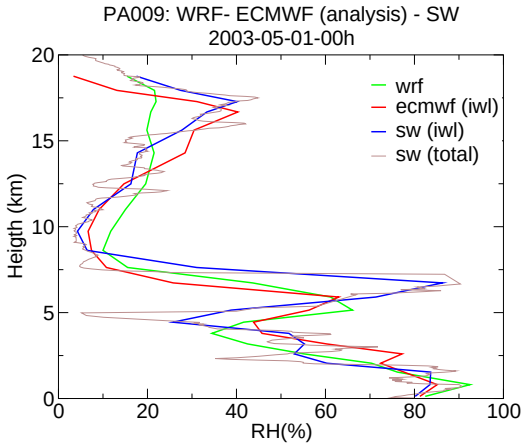

Figure 4.37: As figure 4.29 but on 1 May 2003

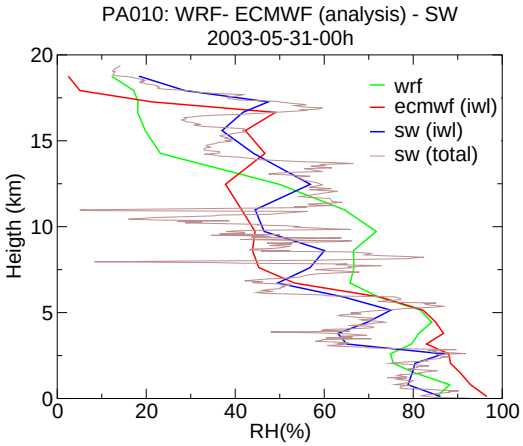

Figure 4.38: As figure 4.29 but on 31 May 2003

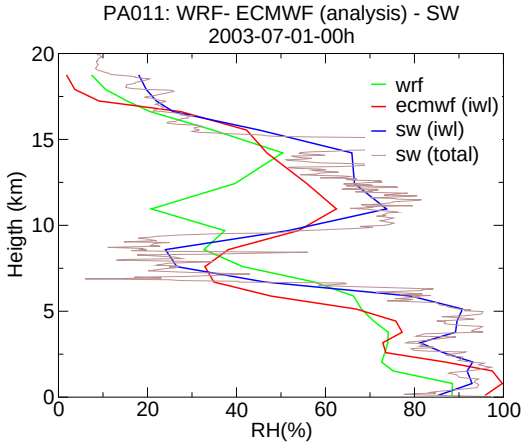

Figure 4.39: As figure 4.29 but on 1 July 2003

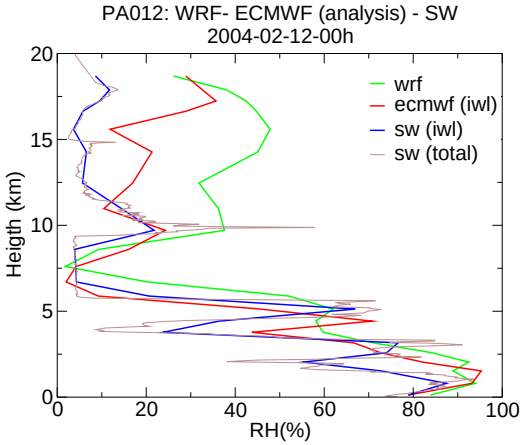

Figure 4.40: As figure 4.29 but on 12 February 2004

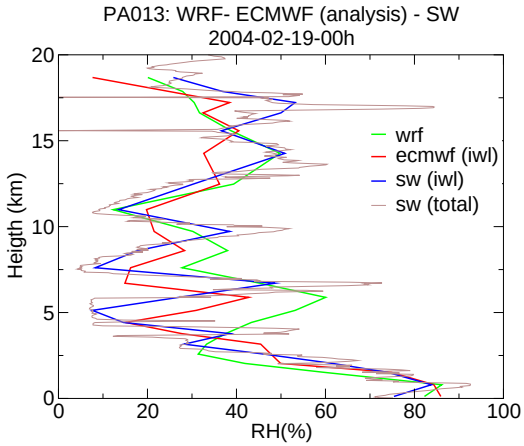

Figure 4.41: As figure 4.29 but on 19 February 2004

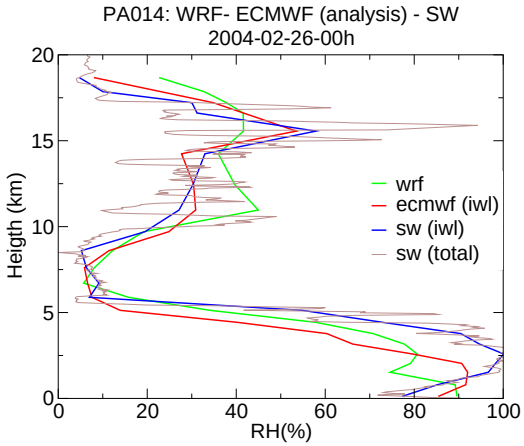

Figure 4.42: As figure 4.29 but on 26 February 2004

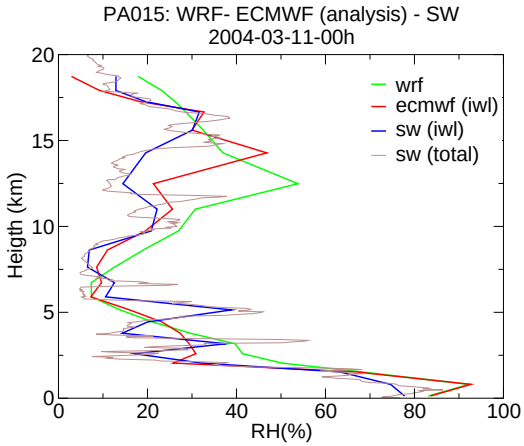

Figure 4.43: As figure 4.29 but on 11 March 2004

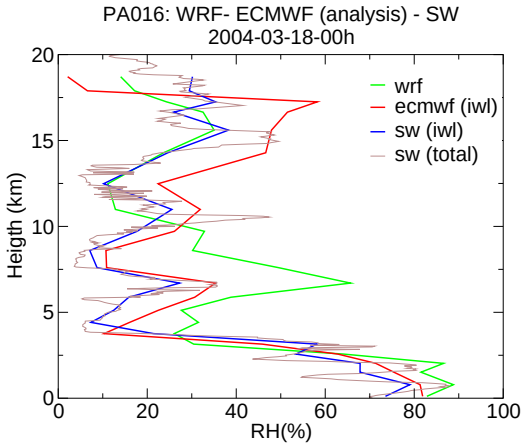

Figure 4.44: As figure 4.29 but on 18 March 2004

A few remarks concerning the SW-observations have to be made. The SW profile of 29 Januari 2003 (pa06, figure 4.34) shows no structure above 5km and stays at very low RH values. The SW sensor did encounter a very dry layer and dried up. After this dry layer the sensor was not able to recover condensate again. this is in accordance with previous observations. [Vöm03]

In two cases pa05 and pa07 (figures 4.33 and 4.35) the observations with SW above 10 km show malfunctions. The measurements show a signal of a SW sensor in total saturation. In the next conclusions about the profiles, we will not consider these three profiles.

A qualitative comparison of the obtained profiles leads to the following conclusions:

- Below 10 km the model profiles agree well with the observations, most structures in the

water vapor distribution are simulated by the modeled profiles.

- Above 10 km there are larger differences with the observations. The models simulate some structures of higher RH values not at the same height as the SW did observe.

A reason for the dislocations e.g. pa03, pa04, pa11, pa15 and pa16, of the higher RH values above 10 km could lie in the fact that the modeled profiles are static in horizontal space. They are all obtained at the location of Paramaribo station whereas the observations did describe a path in the horizontal space and could have measured RH values not at the same point as the models did. Also the fact of the height depended delay time of the SW-sensor results in a shift of the SW-profile (from 0s at the surface up to 80s in the tropopause). [Dol04]

In the next section we will quantitatively investigate the relation between the observations and the modeled profiles. This will be done in terms of a linear correlation between the modeled and the observed profiles.

4.3 Analysis in terms of correlation

To quantify objectively to what extent the modeled water vapor profiles agree with the observations, the statistic of linear correlation is calculated.

Linear correlation is a measure for the degree of coherence between two variables. Two variables are positive correlated when the correlation coefficient is positive and close to 1. In the case of a negative correlation coefficient the two variable are inversely correlated [Spi92]. For a correlation coefficient near zero they are uncorrelated. The correlation coefficient r between two variables X and Y is defined by equation 4.2

$$r = \frac{N\sum XY - (\sum X)(\sum Y)}{\sqrt{[N\sum X^2 - (\sum X)^2][N\sum Y^2 - (\sum Y)^2]}} \tag{4.2}$$

The 95 % significance interval, r_{min} and r_{max} of the correlation coefficient can be computed with equation 4.3.

$$r_{max,min} = \frac{f_{max,min} - 1}{f_{max,min} + 1} \tag{4.3}$$

with $f_{max,min}$ defined by equation 4.4

$$f_{max,min} = \exp(2z + / - 3.92\frac{1}{N-3}) \tag{4.4}$$

and z given by equation 4.5

$$z = \frac{1}{2}\ln(\frac{1+r}{1-r}) \tag{4.5}$$

To determine whether the difference between two nonzero r's, from different experiments e.g. the correlation between the WRF profiles and the observations and the correlation between the ECMWF profiles and the observations, is itself significant, we use the statistic Z:

$$Z = erfc(\frac{|z_1 - z_2|}{\sqrt{2}\sqrt{\frac{1}{N_1-3} + \frac{1}{N_2-3}}}) \tag{4.6}$$

with $z_{1,2}$ the z-coefficient of equation 4.5 for the two samples. Note that Z is normally distributed.

The Fortran programs written to calculate these correlation coefficients and the significances use the correlation subroutines of Numerical Recipes in Fortran 77 [Sof92]. The correlation programs are presented in appendix B.

4.3.1 Correlation between WRF forecasts and observations and between ECMWF analyses and observations

Correlations

The correlation of the modeled and observed profiles has been calculated for the time series (total run) and the vertical distribution. Plots of the 95% significance intervals of the correlation coefficients are presented in appendix A.2.

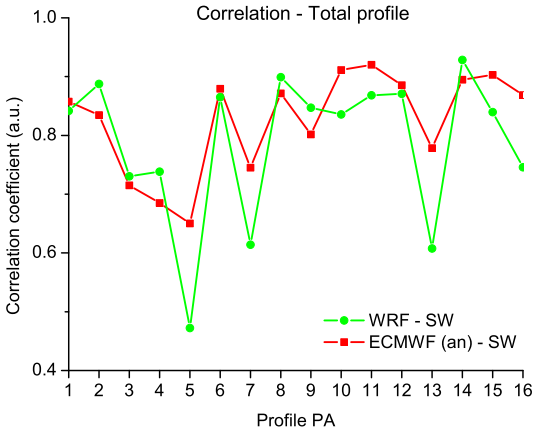

Figure 4.45: Correlation between WRF forecast and observations and between ECMWF analyses and observations for the total profiles

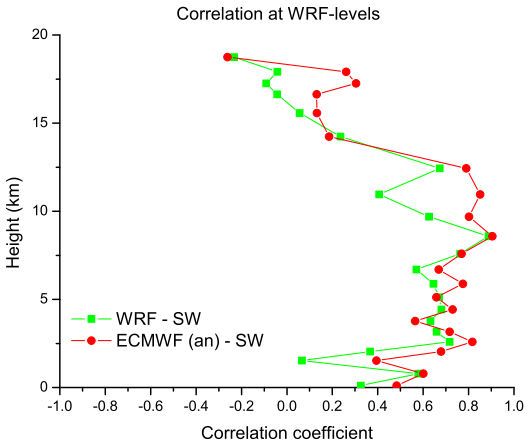

Figure 4.46: Correlation at WRF model levels between WRF 48h FC and observations, and ECMWF analyses and observations

Figure 4.45 shows a strong correlation between the modeled and observed total profiles. Profiles pa05 and p07 show a relatively low correlation this can be explained by the fact of the over saturation of the SW-sensor as mentioned before. In the case of pa06 the correlation is high but the observations show very low RH-values and no structure above 8 km. So this correlation coefficient does not state a thing about the relation between the modeled profiles and the measured values.

Figure 4.46 shows large variations in the values of the correlation coefficients with altitude. Especially towards the tropopause the correlation between the modeled profiles and the observations become weaker and even negative. This level dependent relation between the observations and the simulations in terms of correlation will be further investigated in the next section.

Correlation in parts of the troposphere

Processes in different parts of the troposphere have different implications for water vapor. Boundary layer related phenomena and inflow to deep convective clouds occur in the lowest part of the troposphere, the first 5km. In the middle part of the troposphere, this is the part from 5km till 12km, vertical transport is the main characteristic, and in the upper troposphere and tropopause outflow from convection is and inflow from the stratosphere may become important. Therefore the troposphere is tentatively divided into 3 regions, the boundary layer 0km<z<5km (BL), the middle troposphere 5km<z<12km (MT) and the upper troposphere 12km<z<20km (UT). In these three parts the correlation coefficient is calculated. Next figures 4.47, 4.48 and 4.49 show the correlation in these three parts for the 16 profiles presented in section 4.1.2.

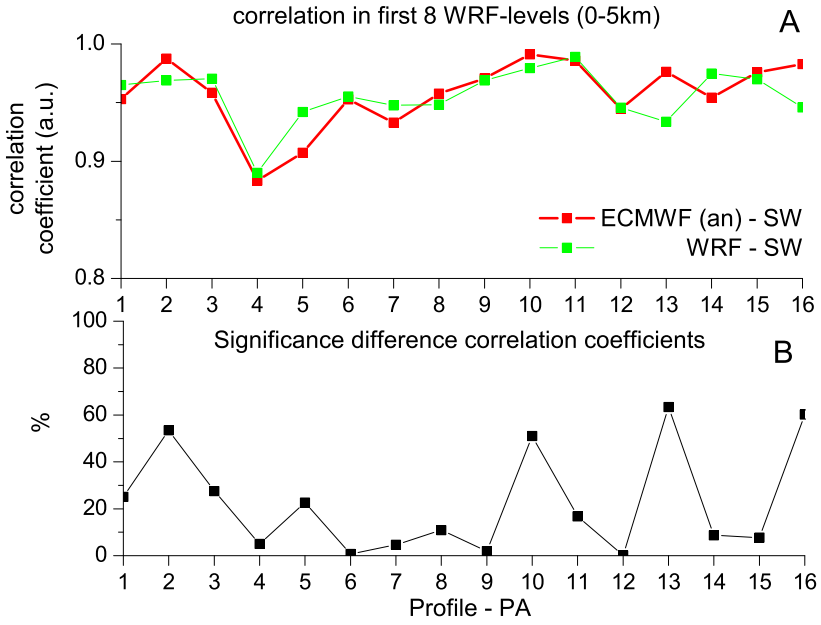

Figure 4.47: **A.** Correlation in the lowest 5 km of the atmosphere at WRF-levels between WRF forecast and observations and between ECMWF analysis and observations, 0km < z < 5 km. **B.** Significance of the difference between the WRF-correlation and ECMWF-correlation.

We see that in the boundary layer, figure 4.47 the correlation coefficients between the two model simulations and the observations are similar and very strong. There are no differences between the two models.

In the middle troposphere and the upper troposphere, the differences become more clear. But these differences between the correlation coefficients vary each profile between the two models. The WRF-model shows sometimes a better correlation (19 out of 32 cases) while in the other cases (13 out of 32) the ECMWF-correlation is greater as the one of the WRF. Thus we can not state that one of the two models preforms better as the other. They seem to do both well.

Also the significance of the differences between the two r coefficients become greater above the first 5 km. But none of the significance values reach the 95% significance interval.

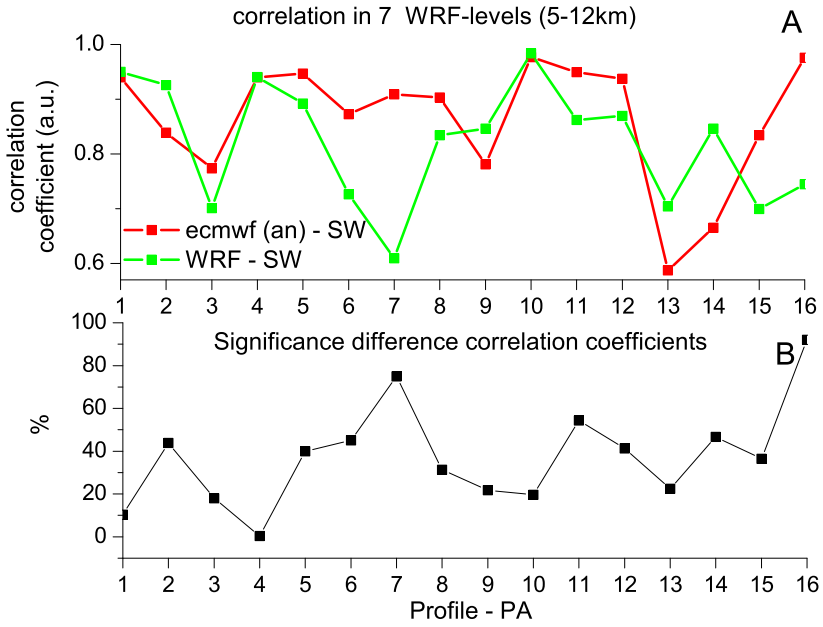

Figure 4.48: **A.** Correlation in the middle troposphere at WRF-levels between WRF forecast and observations and between ECMWF analyses and observations , 5km < z < 12km. **B.** Significance of the difference between the WRF-correlation and ECMWF-correlation.

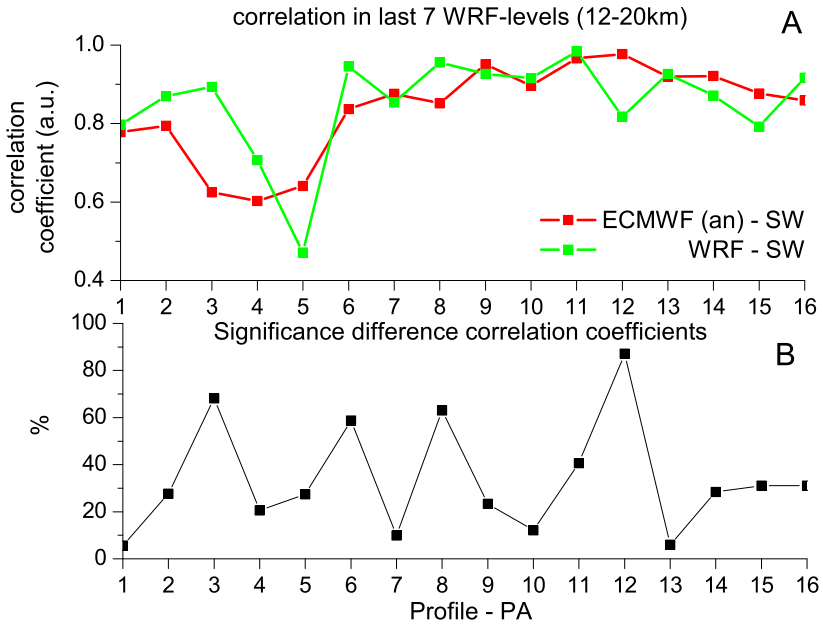

Figure 4.49: **A.** Correlation near the tropopause at WRF-levels between WRF forecast and observations and between ECMWF analyses and observations, 12km < z < 19km. **B.** Significance of the difference between the WRF-correlation and ECMWF-correlation.

4.3.2 Correlation between WRF forecasts and observations and ECMWF forecasts and observations

It would be fairer to compare WRF forecasts with the ECMWF forecasts in stead of ECMWF analyses. The reason is that we would like to determine which model is able to predict best the water vapor distribution. The profiles of the ECMWF forecasts at WRF-levels are presented in appendix A.2.

Correlations

Figures 4.50 and 4.51 show the calculated correlation coefficients between the observed and forecasted profiles.

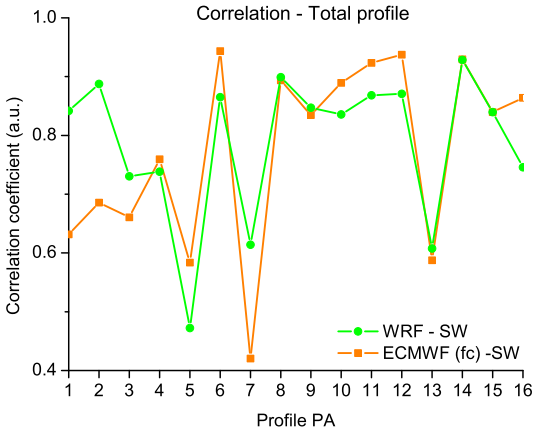

Figure 4.50: Correlation coefficients between forecasted profiles and observations

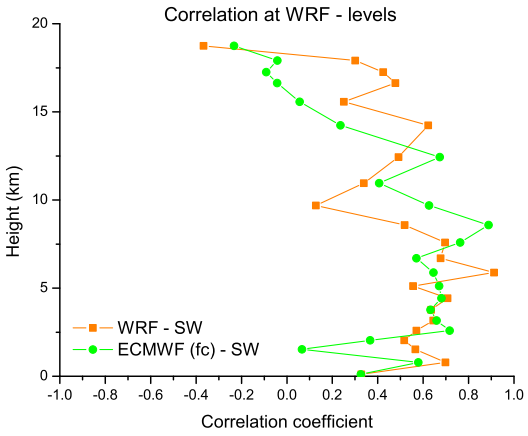

Figure 4.51: Correlation coefficients at WRF model levels between forecasts and observations

Similar to the correlation coefficients calculated between the ECMWF analysis and the observation, the correlation coefficients between the ECMWF forecasts and the observations show weaker correlations at higher altitudes, see figure 4.51. The correlation coefficients of the ECMWF forecasts vary slightly from those of the ECMWF analyses. And smaller than those of the WRF forecasts above about 6 km till 12km and greater than those of the WRF forecasts above 12km. We conclude that the WRF-forecasts perform worse towards higher altitudes than the ECMWF-forecasts.

Correlation in parts of the troposphere

In figures 4.52, 4.53 and 4.54 the correlations in different atmospheric ranges are shown, as well as the significance of the difference between the two model correlations.

It is clear that towards the tropopause the differences between the correlation coefficients become more and more significant. Due to the small number of observations, a conclusion at the 95 % significance level can not be drawn. However, if the number of observations would be increased, it is maybe possible that the difference in the middle upper troposphere will become

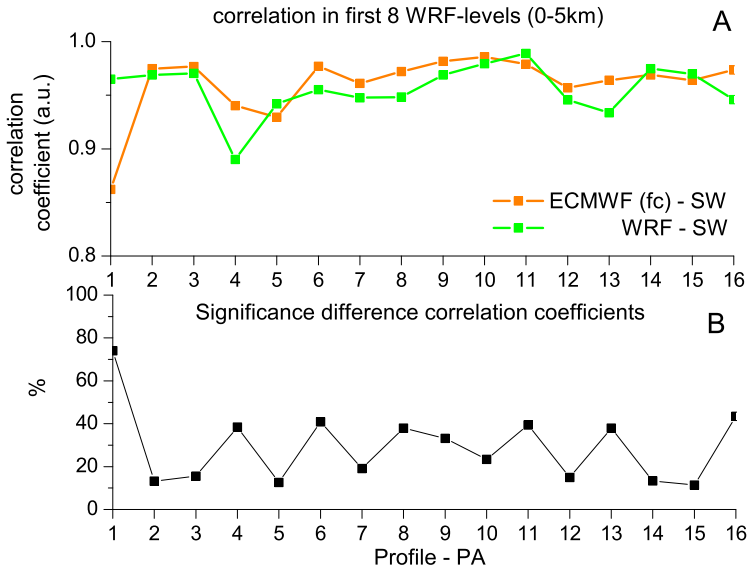

Figure 4.52: **A.** Correlation in the lowest 5 km of the atmosphere at WRF-levels between 48h FC WRF run, ECMWF FC and observations, 0km < Z < 5 km. **B.** Significance of the difference between the WRF-correlation and ECMWF-correlation.

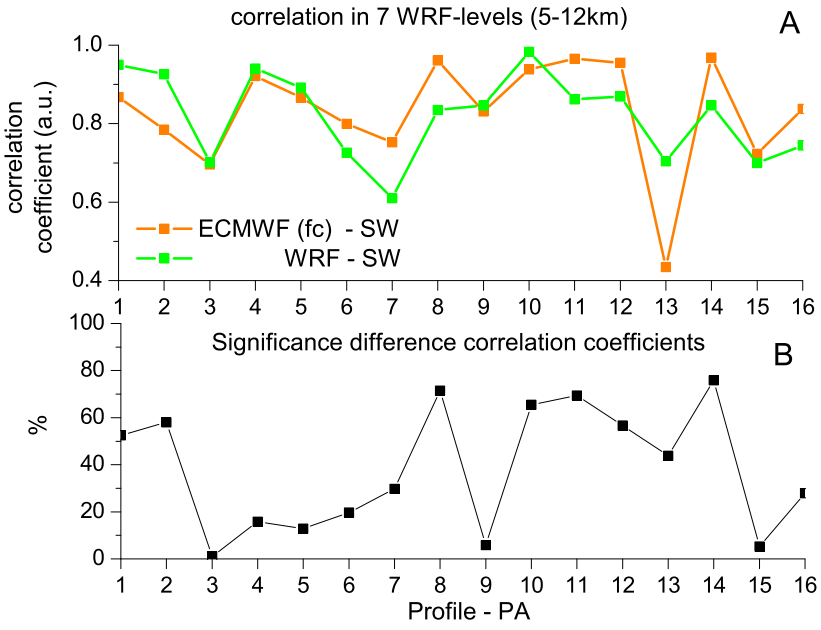

Figure 4.53: **A.** Correlation in the middle troposphere at WRF-levels between 48h FC WRF run, ECMWF FC and observations , 5km < Z < 12km. **B.** Significance of the difference between the WRF-correlation and ECMWF-correlation.

faster significant as in the lower parts of the troposphere. The WRF-forecast preforms as well as

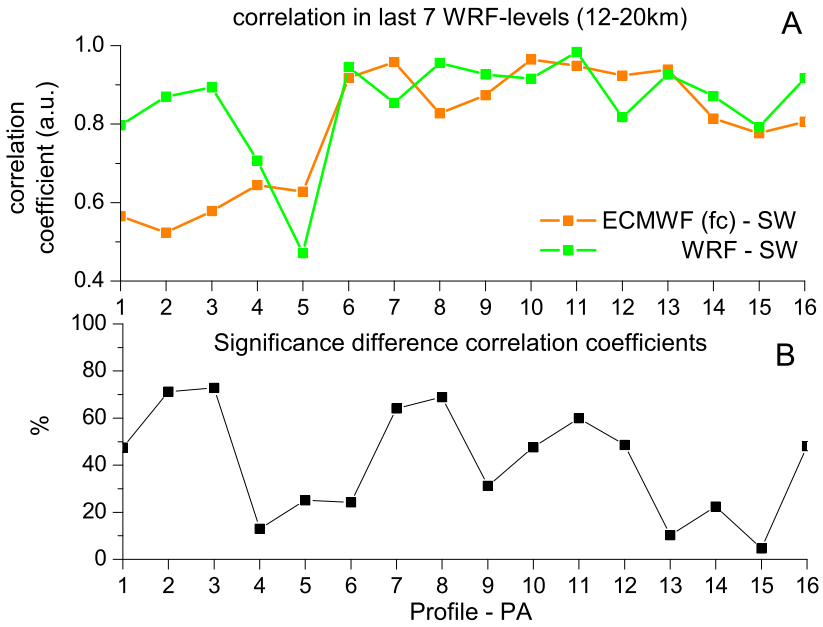

Figure 4.54: **A.** Correlation near the tropopause at WRF-levels between 48h FC WRF run, ECMWF FC and observations, 12km < Z < 19km. **B.** Significance of the difference between the WRF-correlation and ECMWF-correlation.

the ECMWF analysis and forecasts in predicting the water vapor content in the total troposphere.

In order to compare the difference between the WRF correlation and the ECMWF analysis correlation and between the ECMWF forecasts, the mean and median of the significance of the the difference of 13 correlation coefficients in the three parts of the atmosphere are presented in figure 4.55. We used only 13 of the 16 profiles. The profiles Pa05, Pa06 and Pa07 are left out of this analysis because of the malfunction of the SW-sensor above 10km during these 3 measurements.

It is clear that above the first 5km the differences between the correlation coefficients become more significant. The significance of the differences between the correlation coefficients of the WRF forecasts and the ECMWF forecasts is higher (up to 50% in the upper troposphere) than the significance between the WRF forecasts and the ECMWF analysis (30%). Again these significance levels might be increased if the number of experiments would be increased from 16 to e.g. at least 64.

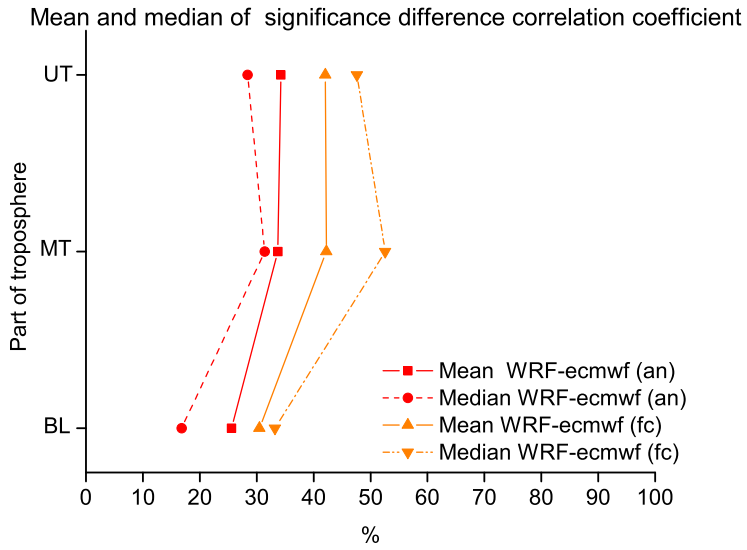

Figure 4.55: Mean and median of the significance of the correlation difference between WRF and ECMWF, analysis and forecasts without PA005, PA006 and PA007.

4.4 Influence of miscellaneous variables on the correlation coefficient

Here we will investigate to what extent the correlation coefficient is influenced by:

- The interpolation of the ECMWF-profile on the vertical WRF levels
- The resolution of the initialization an boundary conditions for the WRF-model input.
- The forecast length of WRF.

,

4.4.1 Influence of interpolation at WRF levels on correlation between ECMWF analyzes and observations

To see to what extent the interpolation of the ECMWF data (38 vertical levels) to the vertical WRF grid (22 levels), influences the correlation between the ECMWF data and the interpolated SW data, a comparison is made between the correlations for interpolation to different numbers of levels.

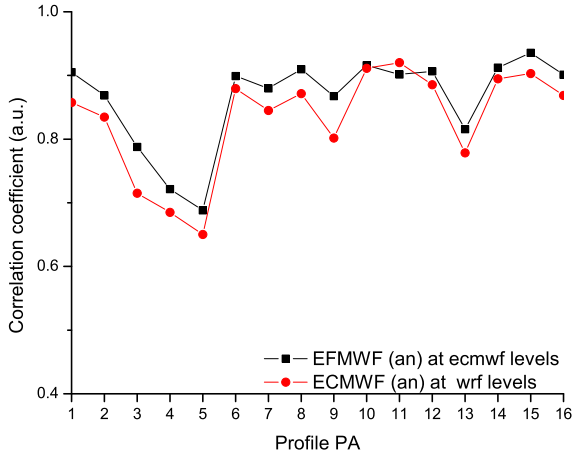

Figure 4.56: Correlation per profile between observations and ECMWF (analyses) profiles at ECMWF levels(38lev) and WRF levels(22lev)

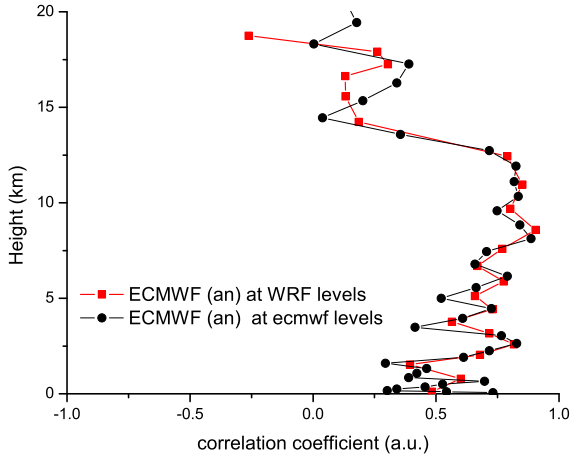

Figure 4.57: Correlation per level between observations and ECMWF (analyses) profiles at ECMWF levels(38lev) and WRF levels (22lev)

The interpolation of the ECMWF-profiles on the WRF-levels only shows a difference in the correlation coefficient at the highest level in figure ??.

4.4.2 Influence of the grid resolution of the boundary values from ECMWF on the WRF simulations

The initial and boundary data, for the WRF runs taken from the ECMWF, are all on the standard ECMWF grid resolution (60kmX60km). The interpolation to the wrf grid (14kmX14km) is done with WRFSI. To investigate the influence of this interpolation and the associated dependence on the resolution of ECMWF data, the same wrf runs were done with boundary and initial data from ECMWF interpolated on a 14kmX14km grid.

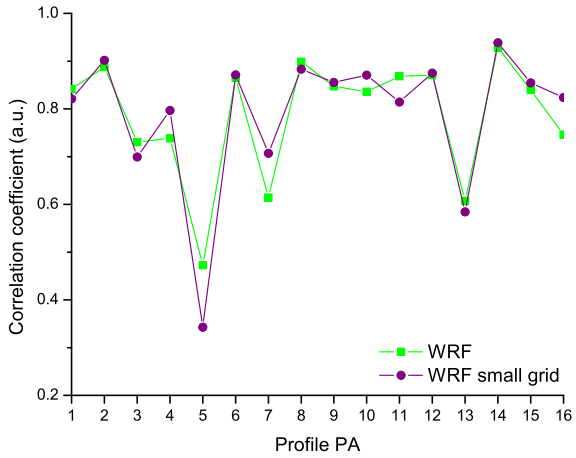

Figure 4.58: Correlation of total run between model data of WRF 48h FC, with large scale and small scale ECMWF input data, and observations

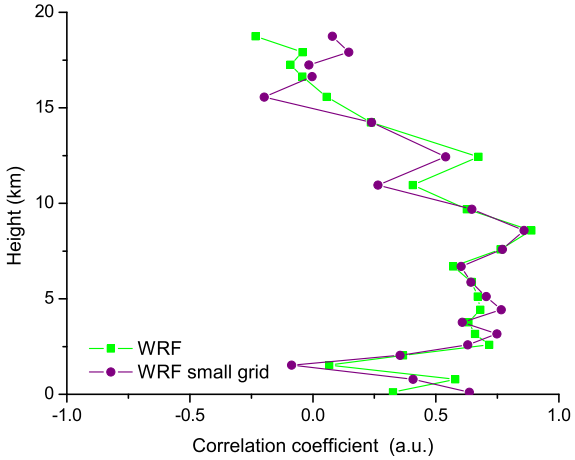

Figure 4.59: Correlation at WRF levels between model data of WRF 48h FC, with large scale and small scale ECMWF input data, and observations

The correlations show minor differences with those obtained with the standard ECMWF grid. Hence the sensitivity to the resolution of the boundary conditions is small.

4.4.3 Dependence of the correlations on the WRF simulation length

In two cases (pa07 and pa13) the total run correlation of WRF show lower values (round 0.60) whereas the other 14 are at least 0.80. To see to what extent the runtime length influences the correlation value, these two runs are done on 3 different forecasting time intervals (simulation lengths) i.e. 24h, 48h and 96h. Figures 4.60 and 4.61 show the WRF forecast profiles with the 3 different time steps and the interpolated SW profile.

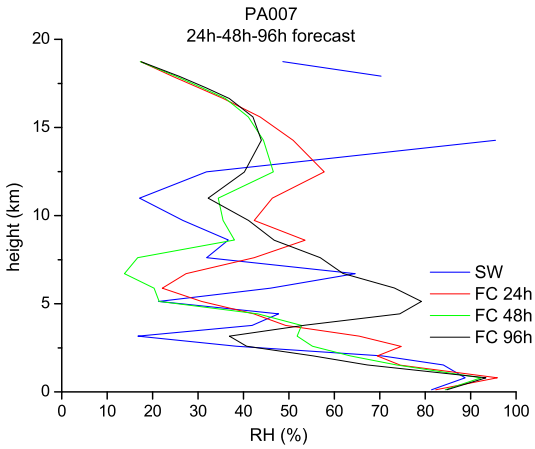

Figure 4.60: profile 7 for 3 different forecast lengths, 24h, 48h and 96h

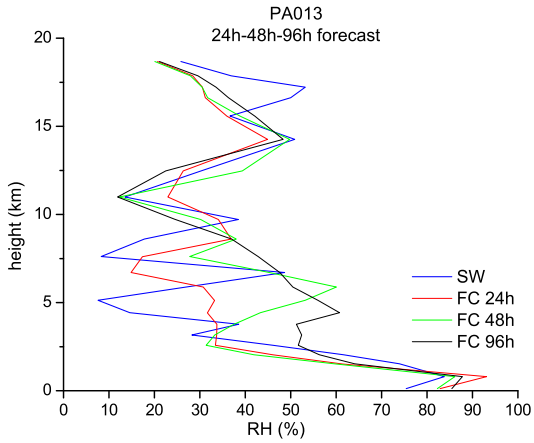

Figure 4.61: profile 13 for 3 different forecast lengths, 24h, 48h and 96h

The calculated correlation coefficients between the WRF simulations with different forecast lengths and the interpolated SW profiles are presented in figure 4.62

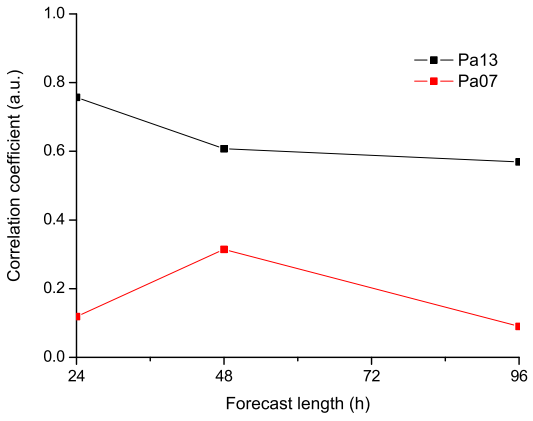

Figure 4.62: Influence of runtime length on correlation between WRF-profile and interpolated SW observations

In both cases the long time run (96h) gives a worse correlation correlation coefficient as the 48h forecast. One case (pa013) has an improved correlation for a short time (24h) run. The other one (pa07) has a lower correlation for the short time run, but we have to keep in mind that the

SW data of pa07 is not totally reliable. It might indicate that a longer forecast length has negative influence on the correlation between the forecast and the observation but we recommend to extend this analysis to more cases.

Chapter 5

Summary and Outlook

5.1 Summary

During this research project the WRF-model was installed and tested. The simulations of the WRF-model give reasonable results. In the case of the RH-profiles at Paramaribo it performs as well as the ECMWF-model forecasts and its analyses. We also found that the coarse resolution of the initial and boundary values does not affect the correlation coefficient between the WRF forecasts and the SW observation much. The influence of the vertical interpolation of the ECMWF also has only minor effects on the correlation coefficient.

5.2 Outlook

More simulations with WRF should be preformed. For instance, the dependence of the difference between observations and model on the forecast length should be further investigated. This should be done for instance above the Netherlands were more meteorological observations are available. If more observations are available one will be able to make a better statistical analysis. Also could WRF be installed and ran at the MDS (Meteo Dienst Suriname) to forecast the RH profiles in advance of a sounding. This to see whether it is useful to do the sounding or not. In the case of the RH-profiles a more detailed study about the observed and simulated structures is recommended to gain more insight in the processes governing these distributions. For instance what is the relation in the water vapor distribution in the upper troposphere and atmospheric waves? WRF is a useful tool for this further research because it is a non-hydrostatic model. Another topic to be investigated is the comparison of the WRF-model with other mesoscale models like HILRAM (the current operational limited area model used at the KNMI).

Acknowledgements

At the end of this thesis I would like to thank a few people without who this all wasn't possible. First of all Dr. Peter van Velthoven for his enthusiastic and enriching supervision. Without your help and motivating discussions there wouldn't be a thesis, thanks. I also have to thank Rinus Scheele very much for his support and debugging skills during the compilation and the first runs of the WRF-model and Mohammed Moustaoui for the introduction to the WRF-model. I would like to thank Prof. Dr. H. Kelder for giving me the opportunity to do this research at the KNMI. Other people of the KS/AS group of KNMI I have to thank are Dr. Ir. Peter Siegmund for the revision of this thesis and the helpful commands and Dr. Gé Verver for the Surinam experience. All by all I own thanks to the whole KS/AS group of the KNMI, for the friendly working environment.

Next to the "professional" people who helped me accomplish this work there are the friends who kept me going. First of all Geert and Thomas, (this is in alphabetical order) thanks guys for having two best friends! Then there are the people of my Diepenbeek time (long time ago but still in the picture) Kim, David, Nico, Bert, Koen, joeri and Kurt we still have to catch that cow!. For the Eindhoven and Utrecht time special thanks go to Hans. At the home front I may not forget lovely Indra, my sisters and of course last but not at least my parents! this one is for you mum and dad!!!!

Bibliography

[BOT99] G. P. Brasseur, J. J. Orlando, and G. S. Tyndall. *Atmospheric chemistry and global change*. Oxford university press, 1999.

[Cur03] J. Curry. *ENCYCLOPEDIA OF ATMOSPHERIC SCIENCES*, chapter Humidity variables, pages 939–941. Elsevier Science, 2003.

[Dol04] Pier Dolmans. Assessment of data quality of water vapor measurements in paramaribo. Tecnical report TR-265, KNMI, de Bilt, The Netherlands, January-March 2004 2004.

[Ely02] B. Ely. Model forecasting. URL: http://www.met.tamu.edu/class/metr452/models/index.html, 2002.

[NCA04] NCAR. modeling system overview. http://www.mmm.ucar.edu/wrf/users/model.html, March 2004.

[Per03] A. Persson. *User guide to ECMWF forecast products*. ECMWF, 3.2 edition, June 2003.

[Pet02] W. Peters. *Ozone in the Tropical Troposphere*. PhD thesis, Universiteit Utrecht, December 2002.

[Pet04] Pete. Numerical weather prediction infaq. URL: http://www.scn.org/ bm733/inFAQ.htm, 11 2004.

[PO92] José P. Peixoto and Abraham H. Oort. *Physics of Climate*. American Institute of Physics, 1992.

[RC91] V. Ramanathan and W. Collins. Thermodynamic regulation of ocean warming by cirrus clouds deduced from observations of the 1987 el ninõ. *Nature*, 351:27–32, May 1991.

[Sal96] M.L. Salby. *Fundamentals of Atmospheric Physics*, volume 61 of *International Geophysics Series*. Academic Press, 1996.

[Sof92] Numerical Recipes Software. *Numerical Recipes in FORTRAN 77: The Art Of Scientific Computing*. Cambridge University Press, 1992.

[Spi92] Murray R. Spiegel. *Theory and problems of statistics*. Shaum's outline series. McGraw-Hill Publishing Company, second edition, 1992.

[UCA04] UCAR. User's guide for weather research and forecast (wrf) modeling system. http://www.mmm.ucar.edu/wrf/users/docs/user_guide/contents.html, March 2004.

[Vöm03] H. Vömel. The behavior of the snow white chilled-mirror hygrometer in extremely dry conditions. *Journal of atmospheric and oceanic technology*, 11:1560–1567, 2003.

[Wal03] D. E. Waliser. *ENCYCLOPEDIA OF ATMOSPHERIC SCIENCES*, chapter Inter Tropical Convergence Zones, pages 2325–2337. Elsevier Science, 2003.

A Results Continued

A.1 ECMWF FC RH fields and profiles

Figures 5.1 up to 5.6 show the wind and RH fields of the ECMWF 48h forecast simulation on 1 March 2003, 00h UTC.

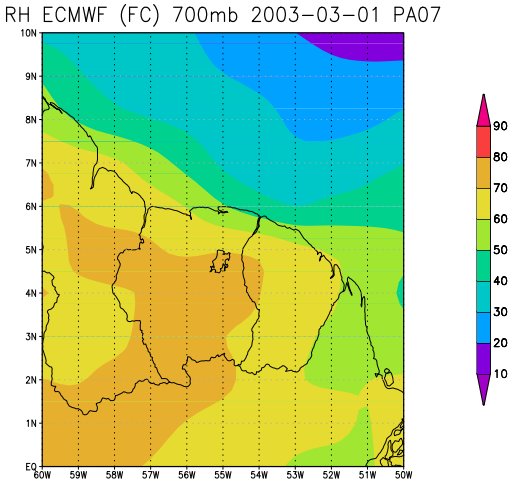

Figure 5.1: RH field at 700mb ECMWF forecast, on 1 March 2003 00h UTC.

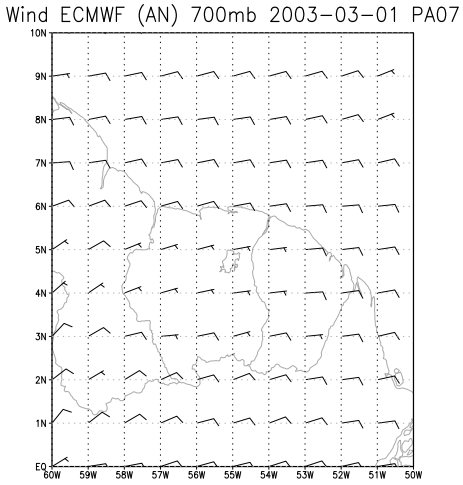

Figure 5.2: Wind field at 700mb ECMWF forecast, on 1 March 2003 00h UTC

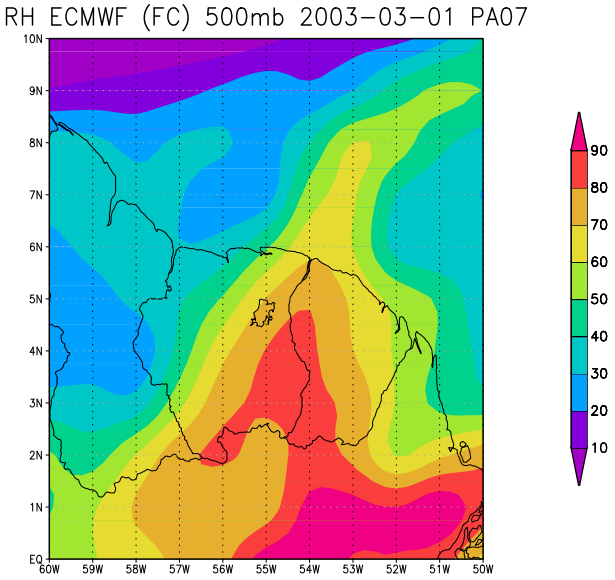

Figure 5.3: RH field at 500mb ECMWF forecast, on 1 March 2003 00h UTC.

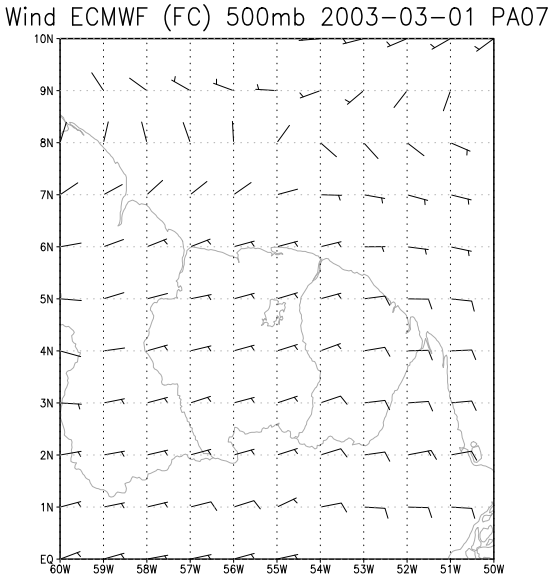

Figure 5.4: Wind field at 500mb ECMWF forecast, on 1 March 2003 00h UTC

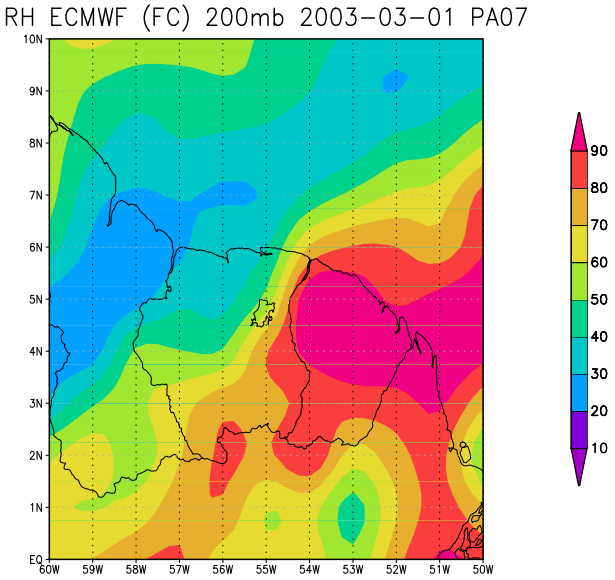

Figure 5.5: RH field at 200mb ECMWF forecast, on 1 March 2003 00h UTC.

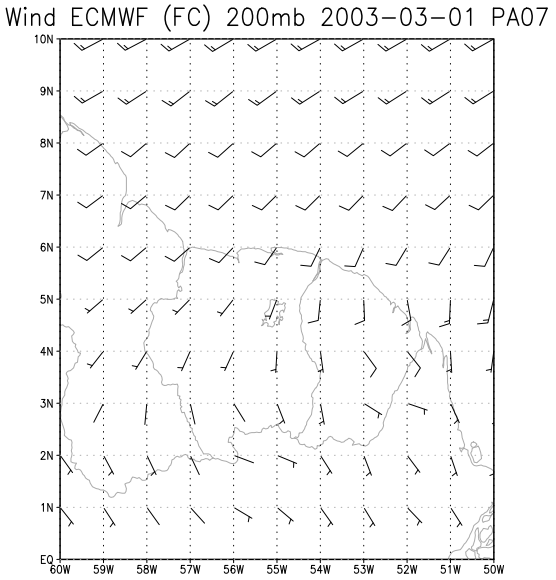

Figure 5.6: Wind field at 200mb ECMWF forecast, on 1 March 2003 00h UTC

Figures 5.7 up to 5.12 show the wind and RH fields of the ECMWF 48h forecast simulation on 26 February 2004, 00h UTC.

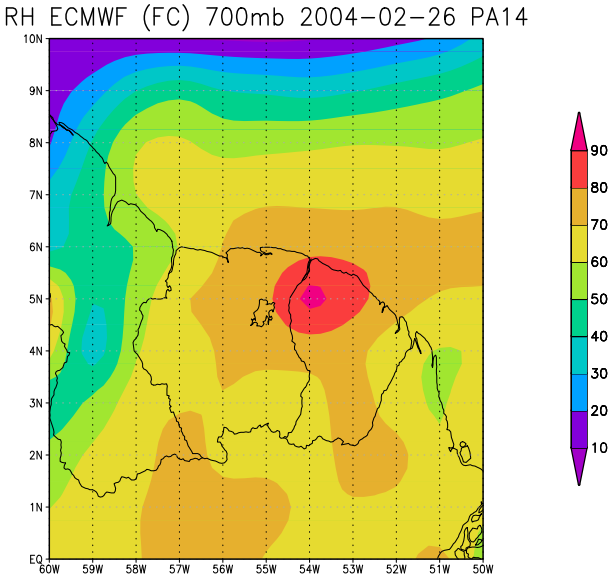

Figure 5.7: RH field at 700mb ECMWF forecast, on 26 February 2004 0h UTC

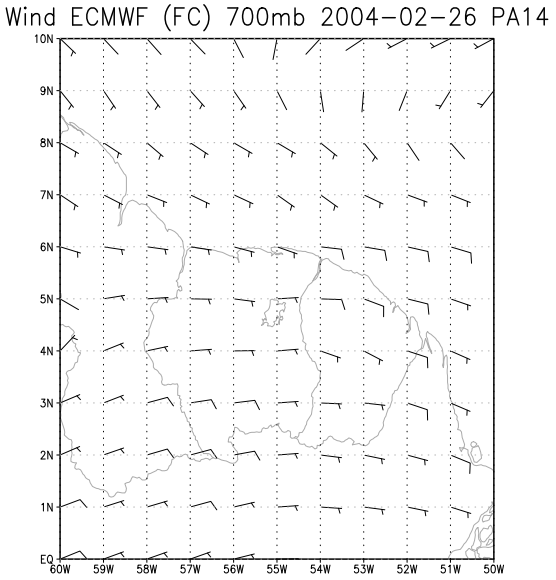

Figure 5.8: Wind field at 700mb ECMWF forecast, on 26 February 2004 00h UTC

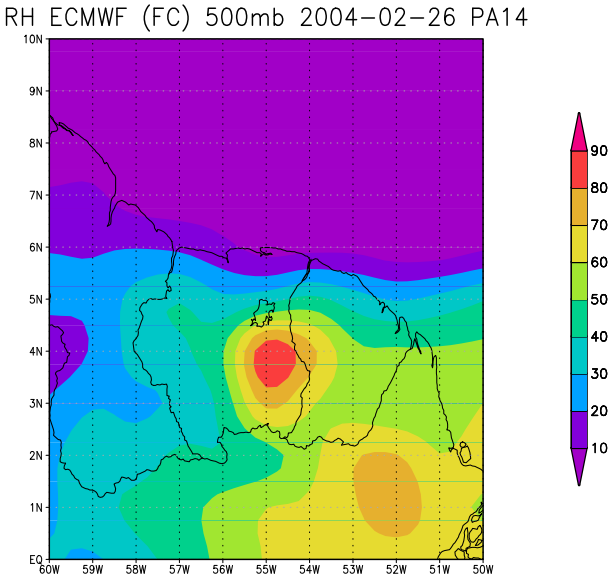

Figure 5.9: RH field at 500mb ECMWF forecast, on 26 February 2004 0h UTC

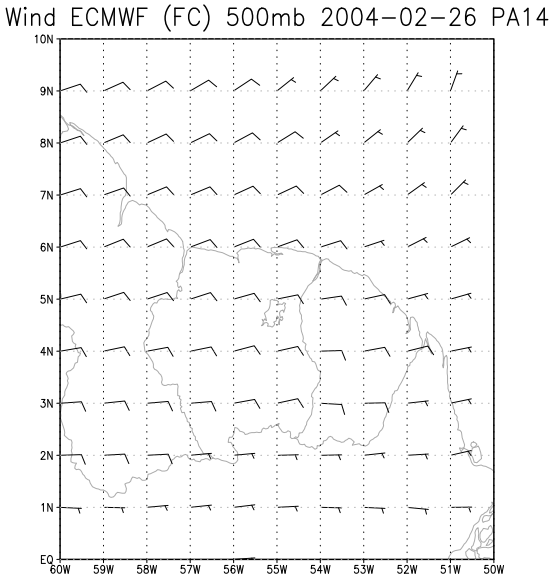

Figure 5.10: Wind field at 500mb ECMWF forecast, on 26 February 2004 00h UTC

Next figure 5.13 shows the 48h ECMWF forecast of high cloud coverage above Surinam.

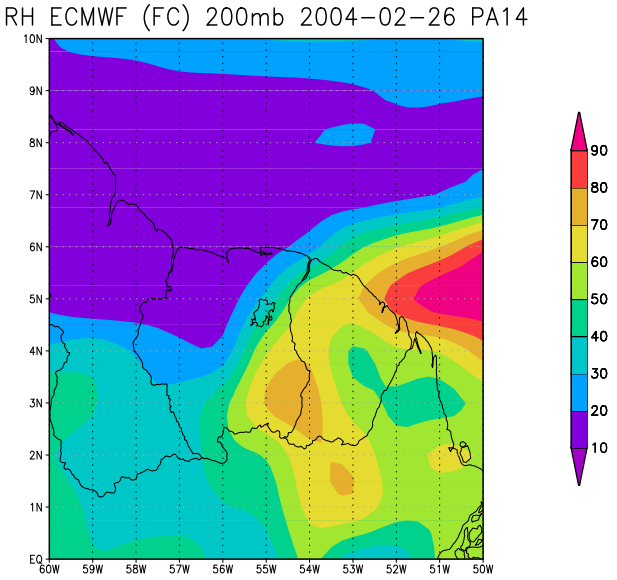

Figure 5.11: RH field at 200mb ECMWF forecast, on 26 February 2004 0h UTC

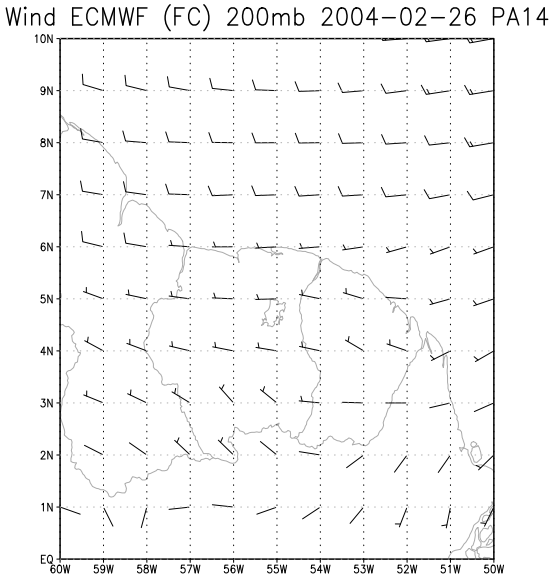

Figure 5.12: Wind field at 200mb ECMWF forecast, on 26 February 2004 00h UTC

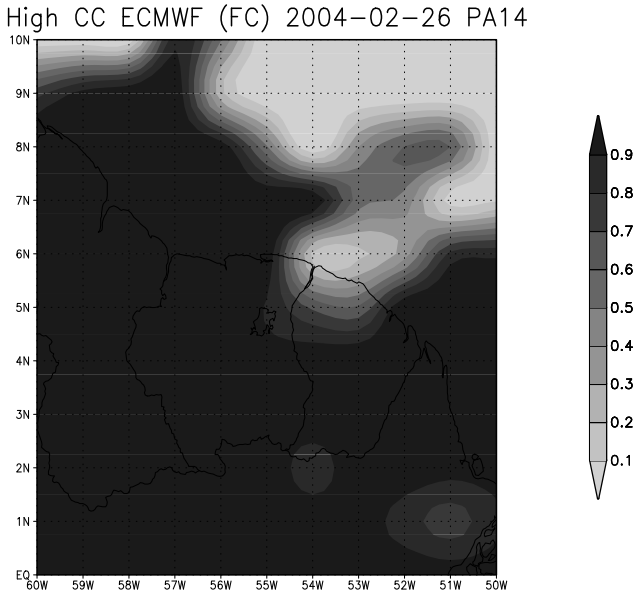

Figure 5.13: The high cloud coverage of the ECMWF 48h forecast on 26 February 2004

The next figures (5.14- 5.29)shown, are the RH profiles at Paramaribo station obtained from the WRF-model (48h forecast), the ECMWF-model (48h forecast) and the SW observations.

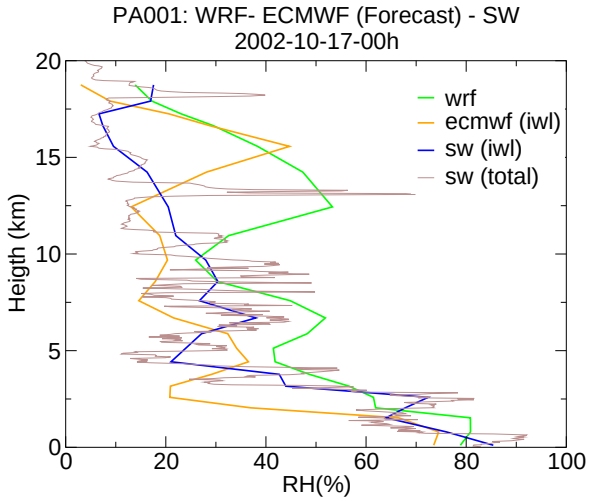

Figure 5.14: profiles of relative humidity at Paramaribo on 17 October 2002 0h UTC from the WRF model (green), ECMWF model forecast (orange) and Snowwhite (blue) interpolated to the WRF model levels, the brown line shows the raw Snowwhite observations

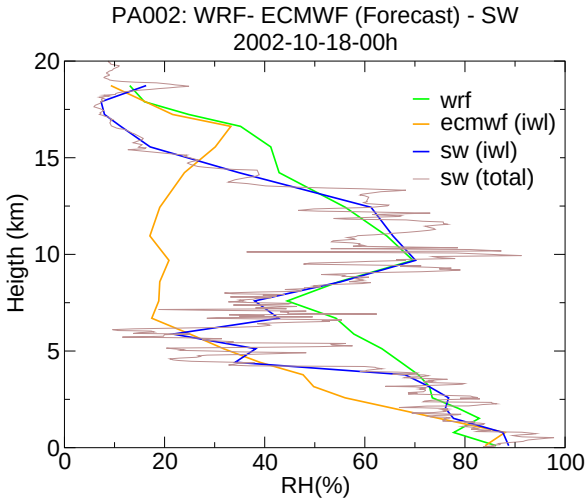

Figure 5.15: As figure 5.14but on 18 October 2002

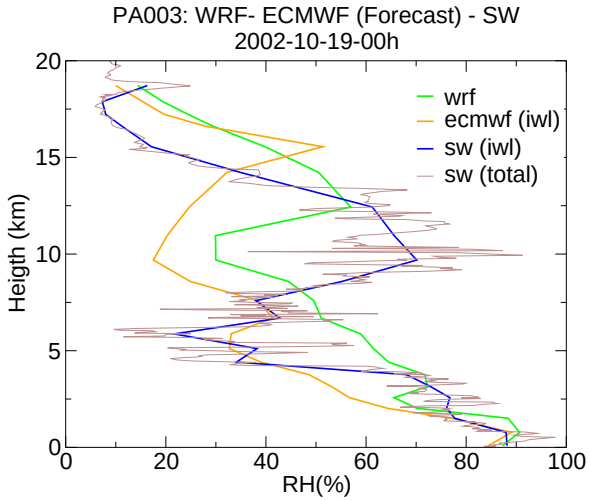

Figure 5.16: As figure 5.14but on 19 October 2002

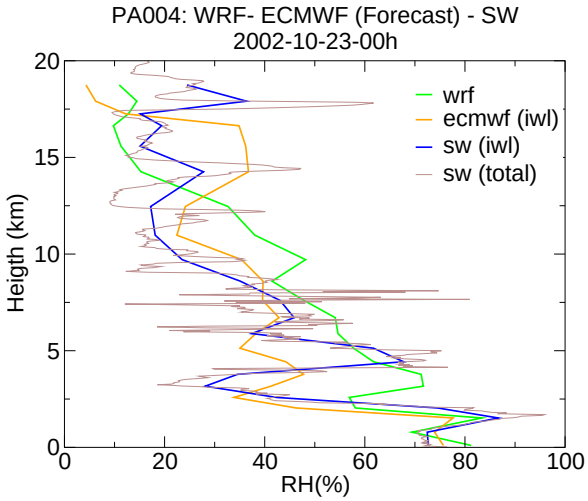

Figure 5.17: As figure 5.14but on 23 October 2002

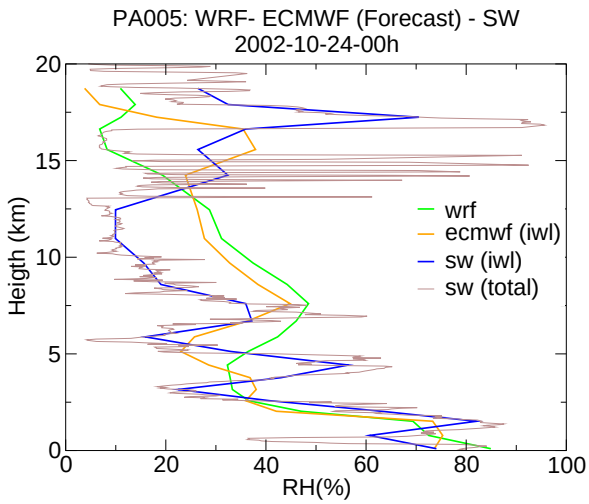

Figure 5.18: As figure 5.14but on 24 October 2002

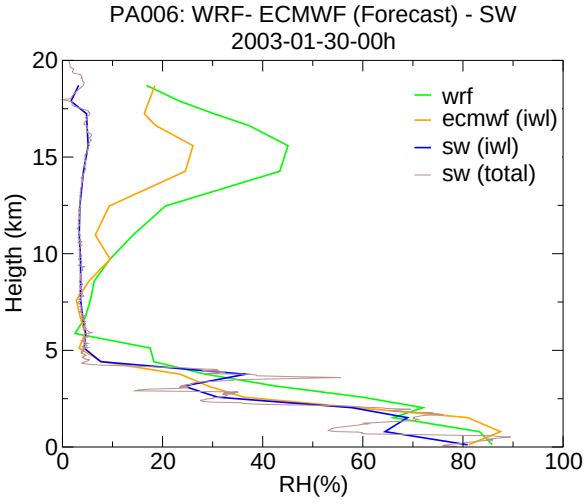

Figure 5.19: As figure 5.14but on 30 Januari 2003

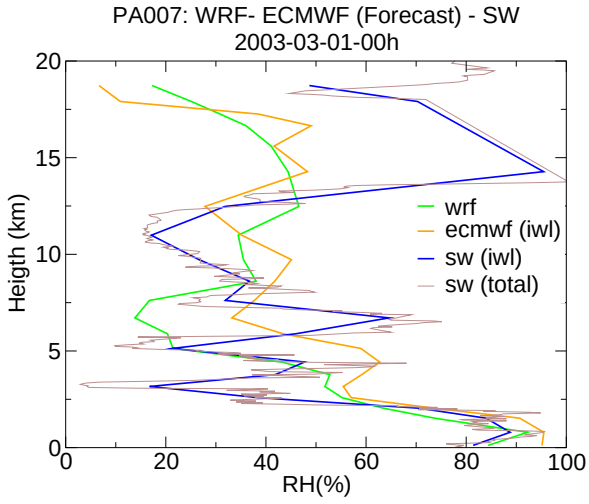

Figure 5.20: As figure 5.14but on 1 March 2003

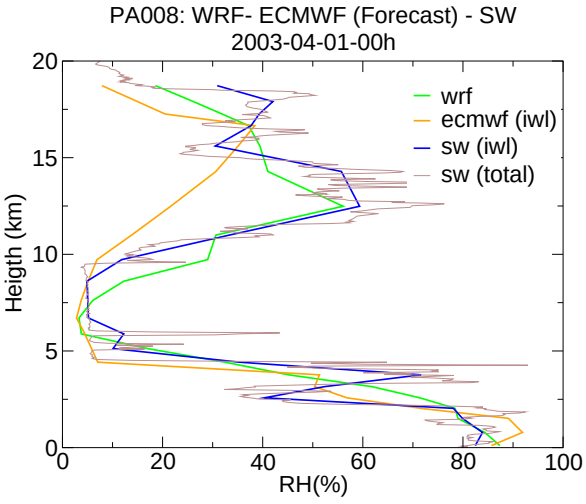

Figure 5.21: As figure 5.14but on 1 April 2003

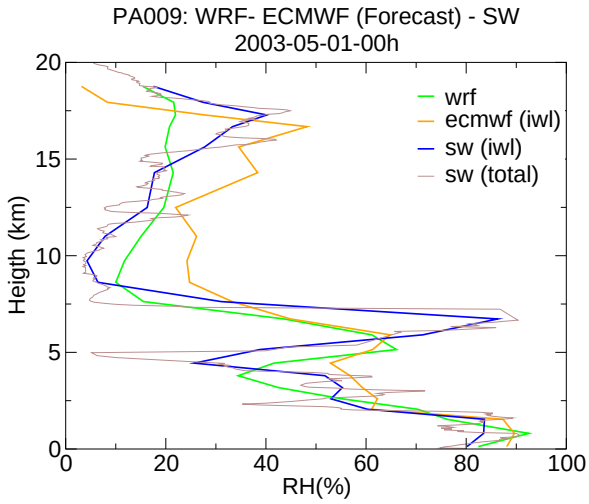

Figure 5.22: As figure 5.14but on 1 May 2003

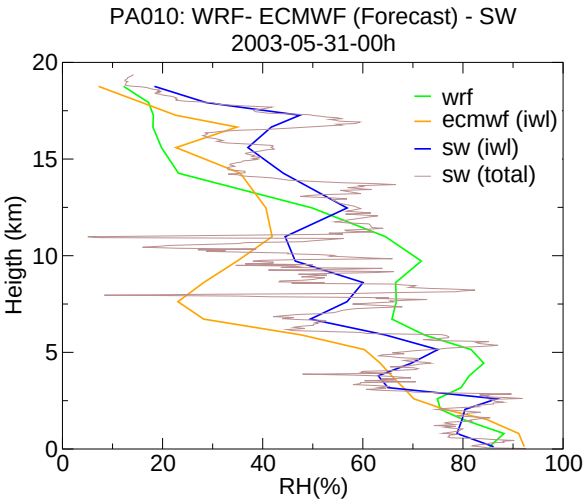

Figure 5.23: As figure 5.14but on 31 May 2003

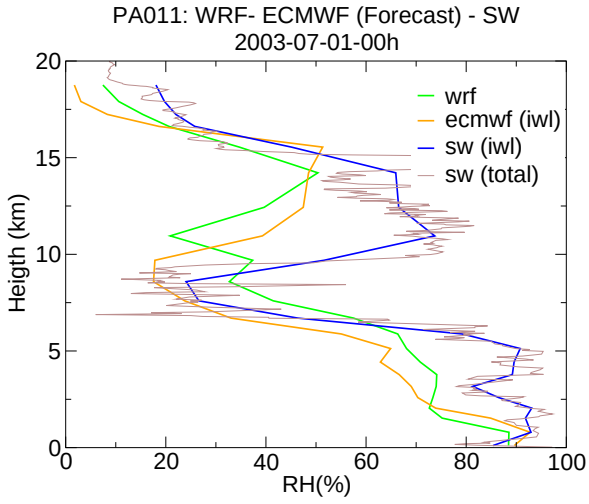

Figure 5.24: As figure 5.14but on 1 July 2003

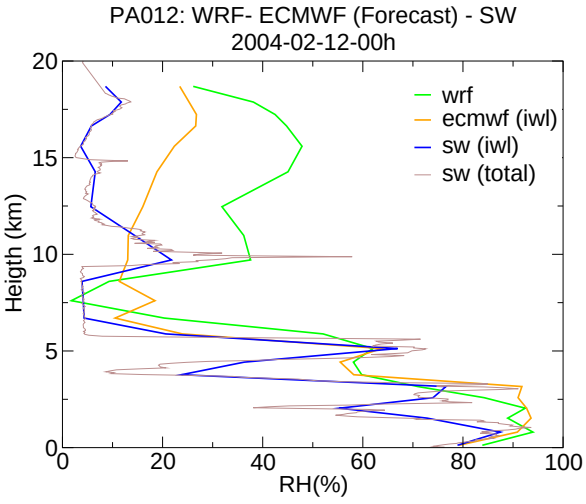

Figure 5.25: As figure 5.14but on 12 February 2004

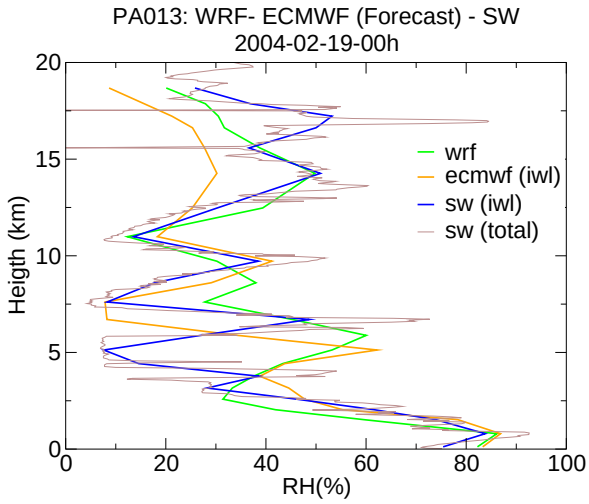

Figure 5.26: As figure 5.14but on 19 February 2004

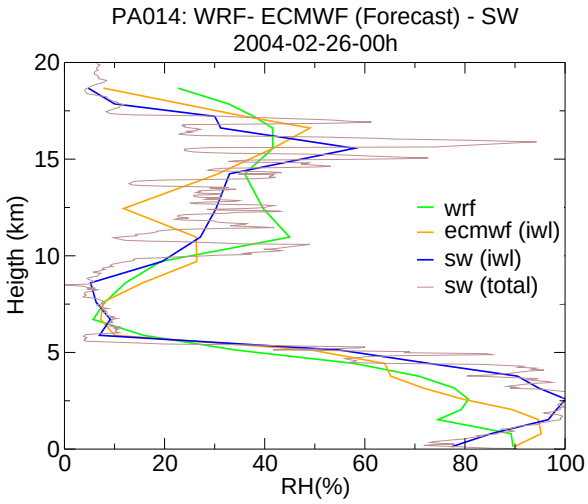

Figure 5.27: As figure 5.14but on 26 February 2004

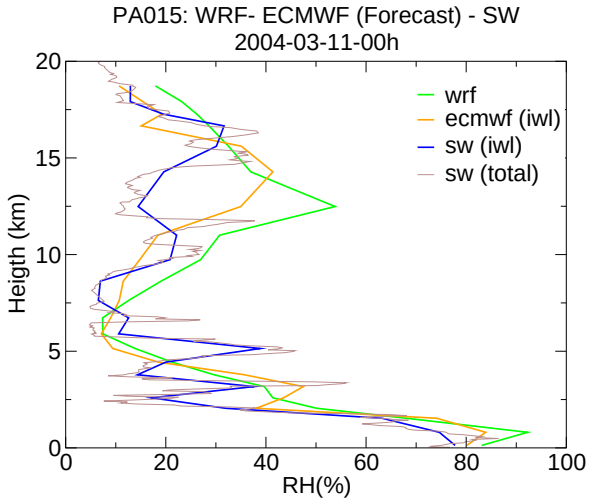

Figure 5.28: As figure 5.14but on 11 March 2004

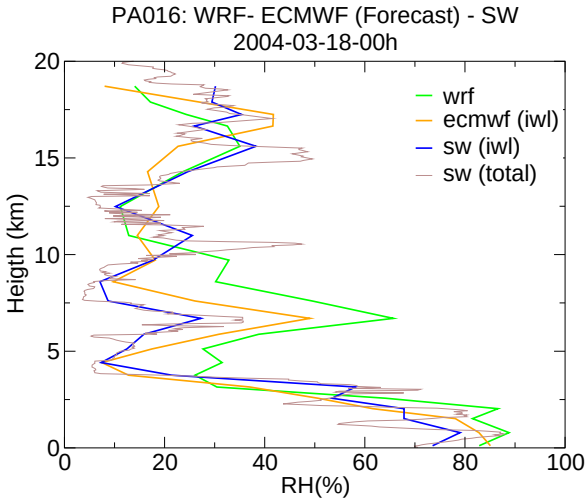

Figure 5.29: As figure 5.14but on 18 March 2004

A.2 Correlation significance plots

In this section the 95% significance intervals of the different correlation coefficients are presented.

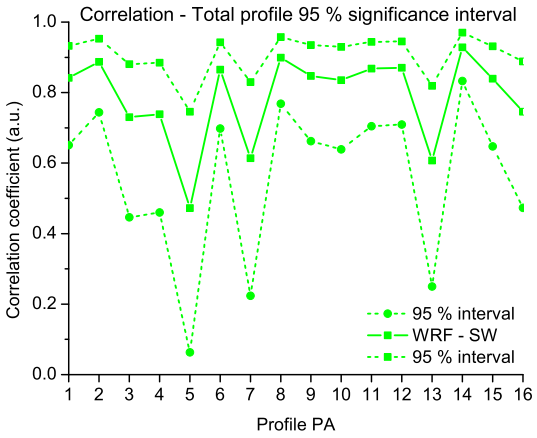

Figure 5.30: 95 % significance interval of correlation coefficient between wrf forecasts and observations

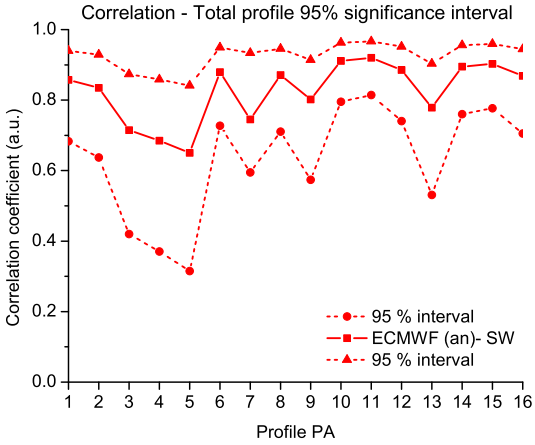

Figure 5.31: 95 % significance interval of correlation coefficient between ecmwf analysis and observations

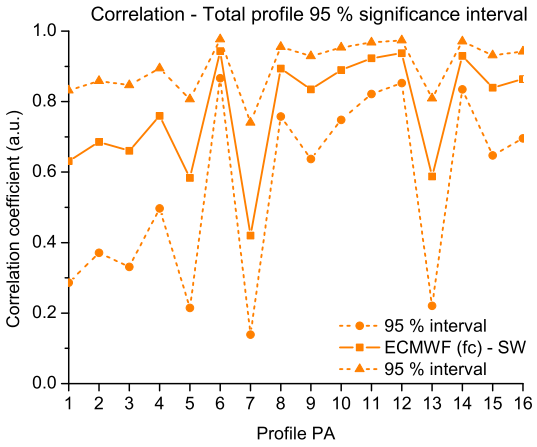

Figure 5.32: 95 % significance interval of correlation coefficient between ecmwf forecasts and observations

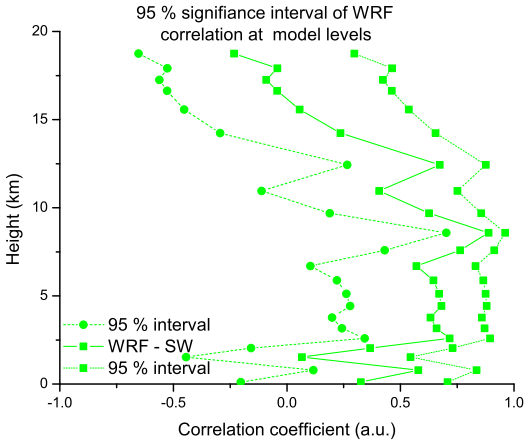

Figure 5.33: 95 % significance interval of correlation coefficient between wrf forecasts and observations at wrf levels

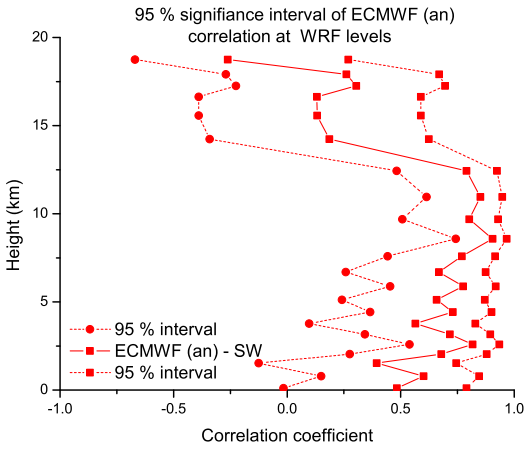

Figure 5.34: 95 % significance interval of correlation coefficient between ecmwf analysis and observations at wrf levels

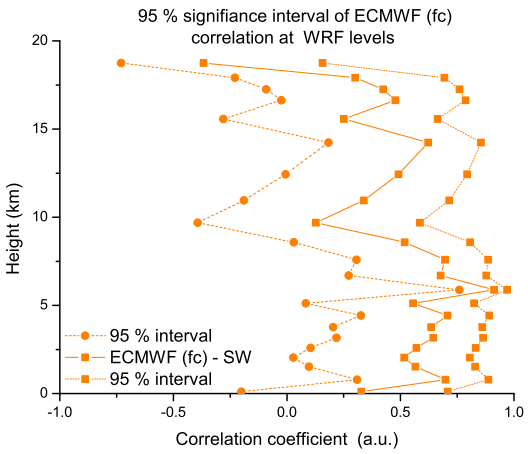

Figure 5.35: 95 % significance interval of correlation coefficient between ecmwf forecasts and observations at wrf levels

B Programs

B.1 Interpolation programs

The two interpolation programs written to interpolate the ECMWF and the SW profiles at the WRF levels are based on equation 4.1. Besides the number of original levels both programs do not differ.

ECMWF Interpolation

*FORTRAN program **EcmIntWrf** interpolates the ECMWF profiles from the original emcwf levels to the 22 WRF levels.*

```
program EcmIntWrf
        implicit none
        integer :: iuin = 12, juin = 13 , iuout = 21
        integer, parameter :: mlev = 22, slev = 922, rn=16
        integer :: imlev, islev, j
        real :: zw(mlev), rhw(mlev), zwbottom(mlev+1)
        real :: ze(slev), rhe(slev), rhew(mlev)
        real :: zb, zt, dz, rhint, dzint
        character*2 rno

        do j = 1, rn
            if (j<=9) then
                write(rno,fmt='("0",I1)') j
            else
                write(rno,fmt='(I2)') j
            end if

            open(iuin, file='Pa'//rno//'.dat', status='old')
            open(juin, file='Ecm'//rno//'.DAT', status='old')
            open(iuout, file='ecmIwrf'//rno//'.DAT', status='unknown')

! read wrfdata
            do imlev = 1, mlev
                read(iuin,*,end =101,err=101) zw(imlev),rhw(imlev)
            end do
101 continue
```

```
        close(iuin)

! Determine the mid-levels (model level boundaries) zmbottom
! First mid-level = surface
! End mid-level = highest model level (so this layer is a bit thin)
        zwbottom(1) = 0
        zwbottom(mlev+1) = zw(mlev)
        do imlev = 2, mlev
            zwbottom(imlev) = (zw(imlev-1)+zw(imlev))*0.5
        end do

! read Ecmdata
        do islev = 1, slev
            read(juin,*,end =100,err=100) ze(islev),rhe(islev)
        end do

100 continue
        close(juin)

! Integrate ecmwflevels between wrf level boundaries
        islev = 1
        zb = 0.
        do imlev = 1, mlev-1
            rhint = 0.
            dzint = 0.
            do
                if (ze(islev).ge.zwbottom(imlev+1)) exit
                zt = (ze(islev)+ze(islev+1)) * 0.5
                dz = (zt-zb)
                rhint = rhint+rhe(islev)*dz
                dzint = dzint + dz
                zb = zt
                islev = islev + 1
            end do
            rhew(imlev) = rhint/dzint
            write(iuout,*) zw(imlev), rhew(imlev)
        end do
        rhew(mlev)=rhe(islev)
        write(iuout,*) zw(mlev), rhew(mlev)

        close(iuout)

    end do

end
```

SW Interpolation

*FORTRAN program **SwIntWrf** interpolates the SW profiles from the original SW levels to the 22 WRF levels.*

```
program SwIntWrf

!Intgerate SWdata on WRFlevels with normal ECMWF grid (2X2)

      implicit none
      integer :: iuin = 12, juin = 13 , iuout = 21
      integer, parameter :: mlev = 22, slev = 922, rn=16
      integer :: imlev, islev, j
      real :: zm(mlev), rhm(mlev), zmbottom(mlev+1)
      real :: zs(slev), rhs(slev), rhsm(mlev)
      real :: zb, zt, dz, rhint, dzint
      character*2 rno

      do j = 1, rn
         if (j<=9) then
            write(rno,fmt='("0",I1)') j
         else
            write(rno,fmt='(I2)') j
         end if

         open(iuin, file='Pa'//rno//'.dat', status='old')
         open(juin, file='sw'//rno//'.DAT', status='old')
         open(iuout, file='swIwrf'//rno//'.DAT', status='unknown')

! read modeldata
         do imlev = 1, mlev
            read(iuin,*,end =101,err=101) zm(imlev),rhm(imlev)
         end do

101 continue
         close(iuin)

! Determine the mid-levels (model level boundaries) zmbottom
! First mid-level = surface
! End mid-level = highest model level (so this layer is a bit thin)
         zmbottom(1) = 0
         zmbottom(mlev+1) = zm(mlev)
         do imlev = 2, mlev
            zmbottom(imlev) = (zm(imlev-1)+zm(imlev))*0.5
         end do

! read SWdata
```

```
        do islev = 1, slev
            read(juin,*,end =100,err=100) zs(islev),rhs(islev)
        end do

100 continue
        close(juin)

! Integrate sonde between model level boundaries
        islev = 1
        zb = 0.
        do imlev = 1, mlev
            rhint = 0.
            dzint = 0.
            do
                if (zs(islev).ge.zmbottom(imlev+1)) exit
                    zt = (zs(islev)+zs(islev+1)) * 0.5
                    dz = (zt-zb)
                    rhint = rhint+rhs(islev)*dz
                    dzint = dzint + dz
                    zb = zt
                    islev = islev + 1
            end do
            rhsm(imlev) = rhint/dzint
                write(iuout,*) zm(imlev), rhsm(imlev)
        end do
        close(iuout)

    end do

end
```

B.2 Correlation programs

The Fortran programs written to calculate the correlation coefficients between the modeled profiles and the observed profiles use the subroutine pearsn from Numerical Recipes in FORTRAN 77 [Sof92].

Correlation program ECMWF-SW

```
program CORRELATIONECMWsign
    implicit none
    integer :: iuin = 12 , juin = 13 , crout = 22 , clout = 23
    integer, parameter :: lev = 22 , rn = 16
    integer :: ilev , irn
    real :: Zwrf(lev,rn) , RHwrf(lev,rn) , Zswint(lev,rn) , RHswint(lev,rn)
    real :: corRU, corZL, tr, tz, Zr, Zl, rhopl, rhomi
```

```
        character*2 rno

        open(crout,file='correcmW.DAT',status='unknown')
        open(clout,file='corlecmW.DAT',status='unknown')

!Read data swint and ecmwf

        do irn = 1, rn
            if (irn<=9) then
                write(rno,fmt='("0",I1)') irn
            else
                write(rno,fmt='(I2)') irn
            end if

            open(iuin, file='ecmIwrf'//rno//'.DAT', status='old')
            open(juin, file='swIwrf'//rno//'.DAT', status='old')

            do ilev = 1, lev
                read(iuin,*,end = 100, err = 100) Zwrf(ilev,irn), RHwrf(ilev,irn)
                read(juin,*,end = 100, err = 100) Zswint(ilev,irn), RHswint(ilev,irn)
            end do

100 continue
            close(iuin)
            close(juin)

        end do

!Calculate correlation between runs
        do irn = 1, rn
            call pearsn(RHwrf(:,irn),RHswint(:,irn),lev,corRU,tr,Zr,rhomi,rhopl)
            write(crout, *),' ',irn, ' ',corRU,' ', rhomi,' ',rhopl
        end do

!Calculate correlation of levels
        do ilev = 1, lev
            call pearsn(RHwrf(ilev,:),RHswint(ilev,:),rn,corZL,tz,Zl,rhomi,rhopl)
            write(clout, *),Zwrf(ilev,1),' ',corZL,' ',rhomi,' ',rhopl
        end do

        close(crout)
        close(clout)

        contains

        subroutine pearsn(x,y,n,r,t,z,rhom,rhop)
            integer:: n
```

```
      real:: r,t,z,rhom,rhop,x(n),y(n)
      real, parameter:: TINY=1.e-20
      integer:: j
      real:: ax,ay,df,sxx,sxy,syy,xt,yt,num,fmi,fpl
      ax=0.
      ay=0.
      do 11 j=1,n
        ax=ax+x(j)
        ay=ay+y(j)
11    continue
      ax=ax/n
      ay=ay/n
      sxx=0.
      syy=0.
      sxy=0.
      do 12 j=1,n
        xt=x(j)-ax
        yt=y(j)-ay
        sxx=sxx+xt**2
        syy=syy+yt**2
        sxy=sxy+xt*yt
12    continue
      r=sxy/sqrt(sxx*syy)
      z=0.5*log(((1.+r)+TINY)/((1.-r)+TINY))
!95% confidence interval
      num=n-3
      fpl=exp(2*z+3.92*(1/SQRT(num)))
      fmi=exp(2*z-3.92*(1/SQRT(num)))
      rhop=(fpl-1)/(fpl+1)
      rhom=(fmi-1)/(fmi+1)
      df=n-2
      t=r*sqrt(df/(((1.-r)+TINY)*((1.+r)+TINY)))
      return
      end subroutine pearsn

end
```

Correlation program WRF-SW

```
program CORRELATIONWRFsign

    implicit none
    integer :: iuin = 12 , juin = 13 , crout = 22 , clout = 23
    integer, parameter :: lev = 22 , rn = 16
    integer :: ilev , irn
    real :: Zwrf(lev,rn) , RHwrf(lev,rn) , Zswint(lev,rn) , RHswint(lev,rn)
    real :: corRU, corZL, tr, tz, Zr, Zl, rhopl, rhomi
```

```
        character*2 rno

        open(crout,file='corrwrf.DAT',status='unknown')
        open(clout,file='corlwrf.DAT',status='unknown')

!Read data swint and wrf

        do irn = 1, rn
            if (irn<=9) then
                write(rno,fmt='("0",I1)') irn
            else
                write(rno,fmt='(I2)') irn
            end if

            open(iuin, file='Pa'//rno//'.dat', status='old')
            open(juin, file='swIwrf'//rno//'.DAT', status='old')

            do ilev = 1, lev
                read(iuin,*,end = 100, err = 100) Zwrf(ilev,irn), RHwrf(ilev,irn)
                read(juin,*,end = 100, err = 100) Zswint(ilev,irn), RHswint(ilev,irn)
            end do

100 continue
            close(iuin)
            close(juin)
        end do

!Calculate correlation between runs
        do irn = 1, rn
            call pearsn(RHwrf(:,irn),RHswint(:,irn),lev,corRU,tr,Zr,rhomi,rhopl)
            write(crout, *),' ',irn, ' ',corRU,' ', rhomi,' ',rhopl
        end do

!Calculate correlation of levels
        do ilev = 1, lev
            call pearsn(RHwrf(ilev,:),RHswint(ilev,:),rn,corZL,tz,Zl,rhomi,rhopl)
            write(clout, *),Zwrf(ilev,1),' ',corZL,' ',rhomi,' ',rhopl
        end do

        close(crout)
        close(clout)

contains
        subroutine pearsn(x,y,n,r,t,z,rhom,rhop)
            integer:: n
            real:: r,t,z,rhom,rhop,x(n),y(n)
            real, parameter:: TINY=1.e-20
```

```
      integer:: j
      real:: ax,ay,df,sxx,sxy,syy,xt,yt,num,fmi,fpl
      ax=0.
      ay=0.
      do 11 j=1,n
        ax=ax+x(j)
        ay=ay+y(j)
11    continue
      ax=ax/n
      ay=ay/n
      sxx=0.
      syy=0.
      sxy=0.
      do 12 j=1,n
        xt=x(j)-ax
        yt=y(j)-ay
        sxx=sxx+xt**2
        syy=syy+yt**2
        sxy=sxy+xt*yt
12    continue
      r=sxy/sqrt(sxx*syy)
      z=0.5*log(((1.+r)+TINY)/((1.-r)+TINY))
!95% confidence interval
      num=n-3
      fpl=exp(2*z+3.92*(1/SQRT(num)))
      fmi=exp(2*z-3.92*(1/SQRT(num)))
      rhop=(fpl-1)/(fpl+1)
      rhom=(fmi-1)/(fmi+1)
      df=n-2
      t=r*sqrt(df/(((1.-r)+TINY)*((1.+r)+TINY)))
      return
      end subroutine pearsn

    end
```

C WRF namelist

The namelist presented here is the being used in all the runs described in this report. The bold and italicized figures are each WRF run adapted for a different run length and case.

```
&namelist_01
        time_step_max= 4560,
        max_dom = 1,
        dyn_opt = 2,
        rk_ord = 3,
        diff_opt = 0,
        km_opt = 1,
        damp_opt = 0,
        isfflx = 1,
        ifsnow = 0,
        icloud = 1,
        num_soil_layers = 5,
        spec_bdy_width = 5,
        spec_zone = 1,
        relax_zone = 4,
        tile_sz_x = 0,
        tile_sz_y = 0,
        numtiles = 1,
        debug_level = 0

&namelist_02
        grid_id = 1,
        level = 1,
        s_we = 1,
        e_we = 90,
        s_sn = 1,
        e_sn = 90,
        s_vert = 1,
        e_vert = 31,
        time_step_count_output = 40,
        frames_per_outfile = 120,
        time_step_count_restart = 0,
        time_step_begin_restart = 0,
        time_step_sound = 8
```

```
&namelist_03
        dx = 14080,
        dy = 14080,
        dt = 90,
        ztop = 19000.,
        zdamp = 5000.,
        dampcoef = 0.2,
        non_hydrostatic = .true.,
        smdiv = 0.1,
        emdiv = 0.01,
        epssm = .1,
        khdif = 0,
        kvdif = 0,
        mix_cr_len = 200.,
        radt = 30,
        bldt = 5,
        cudt = 5,
        julyr = 2001,
        julday = 4,
        gmt = 12.

&namelist_04
        periodic_x = .false.,
        symmetric_xs = .false.,
        symmetric_xe = .false.,
        open_xs = .false.,
        open_xe = .false.,
        periodic_y = .false.,
        symmetric_ys = .false.,
        open_ys = .false.,
        open_ye = .false.,
        nested = .false.,
        specified = .true.,
        top_radiation = .false.,
        chem_opt = 0,
        mp_physics = 3,
        ra_lw_physics = 1,
        ra_sw_physics = 1,
        bl_sfclay_physics = 1,
        bl_surface_physics = 1,
        bl_pbl_physics = 1,
        cu_physics = 1,
        h_mom_adv_order = 5,
        v_mom_adv_order = 3,
        h_sca_adv_order = 5,
        v_sca_adv_order = 3,
```

```
        io_form_history = 2,
        io_form_restart = 2,
        io_form_input = 2,
        io_form_boundary = 2

&namelist_05
        start_year = 2003
        start_month = 02
        start_day = 25
        start_hour = 00
        start_minute = 00,
        start_second = 00,
        end_year = 2003
        end_month = 03
        end_day = 01
        end_hour = 18
        end_minute = 00,
        end_second = 00,
        interval_seconds = 21600
        real_data_init_type = 1

&namelist_quilt
       nio_tasks_per_group = 0,
       nio_groups = 1,
/
```